SUI 63-28

N63 21977

CODE-1

111p.

UNPUBLISHED PRELIMINARY DATA

NSG-233-62

NASA CR51399

OTS PRICE

XEROX $ 9.60ph

MICROFILM $ 3.71mf.

Department of Physics and Astronomy

STATE UNIVERSITY OF IOWA

Iowa City, Iowa

OBSERVATIONS OF INTENSE, LOW ENERGY
ELECTRON FLUXES IN THE OUTER ZONE
DURING JANUARY AND MARCH, 1963*

by

Donald E. Stilwell (M.S. thesis) Aug. 1963 117 p

(NASA CR-51391) OTS: $9.60 ph, $3.71 mf

A thesis submitted in partial fulfillment of the
requirements for the degree of Master of Science
in the Department of Physics and
Astronomy in the Graduate College of the
State University of Iowa State U., Iowa City
4658001

August 1963

Chairman: Assistant Professor H. Leinbach

* Research supported in part by the Office of Naval Research under
Contract N9onr-93803 and by the National Aeronautics and Space
Administration under Grant NsG233-62 and Contract N9onr-93803)
(NASA

ACKNOWLEDGEMENTS

The author is deeply grateful to Dr. Brian J. O'Brien for the suggestion of this research and for his generous understanding and continued interest and guidance throughout the project, to Dr. James A. Van Allen for his liberal support and encouragement, and to Drs. H. Leinbach and D. Venkatesan for their guidance and suggestions during the preparation of this manuscript.

Special thanks are due to Mr. C. D. Laughlin and students and staff members of the Department of Physics and Astronomy for the design and fabrication of the Satellite Injun III as well as for informative and helpful discussions regarding many aspects of this work. Mr. L. Frank supplied the geiger counter modules; Mr. C. Laughlin and Mr. T. Fritz, the spectrometers; Mr. J. Gardner and Mr. H. Taylor, the photometers; Mr. J. Hale, the DC scintillator. Mr. D. Gurnett supplied the satellite electronics as well as the VLF apparatus.

Sincere appreciation is extended to Mrs. Arva Crim who typed the manuscript, to Mrs. Ann DeAntona, and Miss Lona Talbott for their assistance in the compilation of the material reported herein.

This work was supported in part by the Office of Naval Research under Contract N9onr-93803 and by the National Aeronautics and Space Administration under Grant NsG233-62.

ABSTRACT 21977 over

The geophysical research satellite Injun III, containing 18 particle detectors, three auroral photometers, and a VLF experiment, made possible the investigation of the integral electron energy spectrum $J(>E_e)$ (E_e = 10, 40, 100, 250 keV and 1.3 MeV). On four occasions during the months of January and March, 1963, outfluxes from the outer zone at high latitudes were observed to be predominantly electrons and of intensity $j(E_e \geq 10$ keV) $\gtrsim 10^7/\text{cm}^2$ sec sterad. Studies of the integral electron energy spectrum during these intense periods and in the range $4 \lesssim L \lesssim 12$, indicate that on several occasions the integral spectrum in the range $10 \leq E_e \leq 40$ keV does not rise as steeply toward lower energies as does the spectrum in the range $40 \leq E_e \leq 100$ keV. During these occasions, the ratio of flux $J(>10$ keV) / $J(>40$ keV) typically exhibited values between 2 and 20, whereas $J(>40$ keV) / $J(>100$ keV) was observed to lie between 5 and 500. It is suggested that a maximum in the differential electron number-energy spectrum may sometimes exist between $10 \lesssim E_e \lesssim 40$ keV. On occasions when aurorae were also detected by the satellite's photometers, the spectrum

21977

was seen to rise very steeply in the range $10 \leq E_e \leq 40$ keV. Values of $J(>10\ \text{keV}) / J(>40\ \text{keV})$ as high as 1000 were noted. The spectra during any single event were seen to vary widely and rapidly. An electron multiplier responding to electrons of $E_e > 10$ keV was used in the determination of $J(>10\ \text{keV})$. This detector is described in detail.

TABLE OF CONTENTS

TABLE OF TABLES

I. INTRODUCTION

Intense fluxes of low energy (1 keV $\leq E_e \leq$ 50 keV) electrons have been directly observed both within the outer zone [Krasovskii et al., 1961; O'Brien and Laughlin, 1962; O'Brien, 1962b; O'Brien et al., 1962b; Freeman, 1963] and within the northern auroral regions [McIlwain, 1960; Davis et al., 1960; McDiarmid et al., 1961]. The presence of similar electron fluxes outside the earth's magnetosphere has also been reported by Gringauz et al. [1961] and by Freeman [1963]. Measurements of the electron spectra within the outer zone and outside the magnetosphere have frequently been restricted to $E_e \gtrsim 40$ keV. These measurements have indicated that the integral electron energy spectrum rises with no apparent limit toward lower energies, and that the spectrum steepens during intense events. The only measurement within the outer zone (known to this author) which constitutes an indication that the energy spectrum of electrons may not rise without limit is that of Cladis et al. [1961]. They report a determination of the energy spectrum by a rocket-borne spectrometer in the inner edge of the outer zone during a single traversal at $\sim$1000 km altitude. The observation indicates that a maximum in the differential electron energy distribution function of electrons of energy $E_e \gtrsim 50$ keV may exist at $E_e \sim 70$ keV. The L value of this measurement was $L \sim 2.4$.

Measurements of electron spectra within visual aurorae, which have been reported in the afore cited references, indicate that the average energy of auroral electrons is generally between 5 and 20 keV. McIlwain [1960] observed a differential electron number-energy distribution which displayed maxima at 7 and 11 keV during two separate events. The other measurements utilized atmospheric absorption during rocket ascent and descent to obtain energy spectra. These latter determinations displayed no apparent differential maxima, but indicated generally soft spectra.

O'Brien et al. [1962a] have recently reported that large outfluxes of electrons from the outer zone with intensities $j(E_e \geq 40 \text{ keV}) \approx 10^5/\text{cm}^2$ sec sterad may be observed frequently at auroral latitudes. The source of these electrons is unknown, but it appears certain that they can not be derived completely from trapped fluxes observed at satellite altitudes [O'Brien, 1962a]. Among the possible sources (for these and other mechanisms, see Kaufman [1963]) to be considered are (a) these electrons are present throughout the magnetosphere with thermal energies and may be accelerated to energies of a few tens of keV to be injected into precipitating orbits, (b) these electrons are present as high energy particles which are shortlived residents of the outer zone, and which undergo energy degradation to eventually become precipitated, or (c) these electrons are derived, with or without energy modification, wholly from outside the magnetosphere, to be temporarily trapped and later precipitated, or to execute less than a single latitudinal oscillation and thus to be lost immediately. It would be desirable, therefore, to know the detailed nature of the low energy electron fluxes and spectra within the outer zone during both quiet and disturbed periods. However, the "exact fluxes of low energy particles are completely uncertain" [O'Brien, 1963c].

It is the purpose of this research to investigate the integral energy spectrum of electrons of $E_e \gtrsim 10$ keV during intense events at high latitudes utilizing instrumentation aboard the Injun III satellite. An open-ended electron multiplier structure for the detection of 10 keV electrons will be described. Four periods of geomagnetic disturbance in the months of January and March, 1963, during which high fluxes of electrons were observed within the outer zone are selected for study. It will be shown that on several occasions the differential electron distribution function does display an apparent maximum in the range 10 keV $\leq E_e \leq$ 40 keV, but that the spectral form is highly variable both during a single event and from one event to another.

II. DESCRIPTION OF THE SATELLITE

Injun III was designed to provide an integrated set of detection apparatus to investigate the dynamics and structure of the radiation zones and particularly the relation of the outer zone to the occurrence of certain high latitude phenomena such as aurora, airglow, VLF emissions, and ionospheric disturbances. The instrumentation includes 18 particle detectors, three auroral and airglow photometers to measure light of 5577Å oxygen line and the 3914Å N_2 band, and a VLF receiver to analyze electromagnetic emissions in the range of frequencies from 500 cps to 7 Kcps. The outputs of most detectors (except the VLF and the PN-junction proton detectors) are sampled at intervals of 1/4 second each thus providing a time resolution corresponding to less than 2 kilometers along the satellite trajectory. Each such sample is uniquely labeled by two on-board digital clocks, designated by the letters A and B.

Satellite Injun III (1962 beta-tau) was launched December 13, 1962 into an elliptical orbit inclined at 70.4° to the geographic equator. The initial orbital parameters of significance in our study are

Apogee altitude	-	2785 km
Perigee altitude	-	237 km
Period	-	116 minutes

The eccentricity of the orbit, although not intended, is beneficial in the respect that during each revolution, a profile of L space to L values as high as ~ 50 may be obtained at high latitudes.

Charged particles travelling within the geomagnetic field spiral about the magnetic field lines. The pitch angle between the local $\underline{B}$ vector and the velocity vector of a given particle is known as the pitch angle α of that particle, and the flux at any given pitch angle is essentially independent of the azimuthal angle about the field line. A permanent magnet installed in Injun III orients the satellite with one axis parallel to the local $\underline{B}$ vector. Each of the particle detectors are oriented at an angle θ to this axis of alignment, and hence respond to particles of a known pitch angle. $\theta = 0^{\circ}$ is defined as being directed downward in the northern hemisphere. Orientation of the satellite with respect to the local $\underline{B}$ vector may be determined with two flux gate magnetometers which are oriented such that the axis of sensitivity of each is directed at $\theta = 90^{\circ}$ and 130° respectively. The first of these is therefore sensitive only to the component of the local field perpendicular to the axis of alignment. Thus, at perfect alignment, this determination is independent of the scalar value of local $\underline{B}$. The second magnetometer determines the component of $\underline{B}$ directed at an angle of 130° to the axis of alignment. Therefore, if the scalar value of $\underline{B}$ at the satellite is known, this magnetometer provides a measure of the angle between the direction of B and the sensitive axis of the magnetometer.

It is possible to obtain limited information regarding the orientation of the satellite with respect to the sun from five solar aspect sensors. These were designed to detect the presence of the solar disc within the viewing cone of selected groups of detectors. The location and angular fields of view [Laughlin, private communication] of these sensors are given in Table I.

A detailed description of the Injun III detector complement has been given by O'Brien et al. [1963] which is summarized in Table I. Figure 1 is a plan-view photo of the satellite illustrating the orientation of all detectors with respect to B. It is pertinent at this point to review certain aspects of the instrumentation in light of the goals of the present investigation.

The parameters of primary interest in this study of the intense events at high latitudes are (a) the energy spectra of both precipitated and trapped particles, (b) the angular distribution of these particles about the local B vector, and (c) the relation of these parameters to associated high latitude phenomenon, specifically aurora, airglow, and VLF emissions. It will also be of interest to note several features of the spatial and/or temporal structure of the outer zone during such events.

The detectors of principal concern, then, are the 213 geiger counters, the differential magnetic electron spectrometer, the integral electron spectrometer, the DC scintillator, and the electron multiplier. The properties of this latter detector will be described in some detail in the following section; a brief description of the others will be given here. We will also be concerned with the qualitative response of the photometric and the VLF apparatus, but need not for the present delve into the instrumental aspects of these detectors. We will consider each a black box which indicates the presence of the phenomenon they are designed to detect.

A. Geiger Counters.

There are five of these detectors, designated by the letters A - D, which utilize Anton type 213 geiger tubes. Geigers 213A and 213C are thin-windowed ($\sim$1.2 mg/cm^2 mica) directional detectors oriented at 90° and 130° respectively to the local $\underline{B}$ vector. The threshold for detection by direct penetration is $\sim$40 keV for electrons and $\sim$500 keV for protons. The angular field of view of each is $\sim$26° in diameter, and the geometric factors are 0.6 x 10^{-2} and 1.1 x 10^{-2} cm^2 sterad respectively.

The 213B is identical in all respects to 213A except that the window thickness has been increased by an additional 45 mg/cm^2 of aluminum and that the geometric factor is $\sim 10^{-2}$ cm^2 sterad. The corresponding threshold for electrons is 250 keV and 4 MeV for protons.

The 213D is similar to 213A but is oriented at 180° to the field, the angular field of view is 86° in diameter, and the geometric factor is 5×10^{-2} cm^2 sterad. All geigers are shielded by 3 g $/cm^2$ of lead and stainless steel except over their apertures.

B. Differential Spectrometer.

This instrument, oriented at $\theta = 90^{\circ}$, utilizes two magnets to focus electrons of energy $42 \leq E_e \leq 53$ keV and $83 \leq E_e \leq 98$ keV into two type 213 geiger tubes contained within a lead cylinder 3.5 g/cm^2 in thickness except over the aperture. These two channels will be designated SpL and SpH respectively. A third 213 is also contained within this cylinder, but is shielded in all directions. This serves as a background detector for the detection of penetrating particles and bremsstrahlung produced in the housing and satellite skin, and is designated SpB. The directional geometric factors of the low (SpL) and high (SpH) channels are 2.3×10^{-4} and 3.0×10^{-4} cm^2 sterad respectively, the omnidirectional geometric factor of the background counter is about 0.2 cm^2.

C. Integral Spectrometer.

The integral spectrometer also utilizes three type 213 geiger counters, one of which serves as a background counter as in the differential unit described above. The other two tubes, designated IsL and IsH, are placed behind separate apertures containing magnetic brooms to sweep away electrons of energy $E_e \lesssim 1.3$ MeV and $E_e \lesssim 3.0$ MeV respectively. The directional geometric factor of each is approximately 10^{-2} cm^2 sterad.

D. DC Scintillator.

The DC scintillator is an integrating device responding to the total energy flux incident on a disc of CsI approximately 20 mg/cm^2 in thickness. It will be designated here by DC.

The crystal is covered by 86 $\mu g/cm^2$ nickel foil to attenuate incident sunlight falling on the photomultiplier cathode by a factor of $\sim 10^5$. The foil thickness corresponds in range to particle energies for direct penetration of $E_e \sim 5$ keV for electrons and $E_p \sim 50$ keV for protons. The detector is oriented at 130^o with respect to $\underline{B}$, and has an angular field of view about 20^o in diameter. The geometric factor is 1.4×10^{-2} cm^2 sterad. Due to an as yet unexplained malfunction, the sensitivity of this detector has degraded since preflight calibration by about a factor of 8 to 10. Hence, the response of this detector will be used only in a differential sense to indicate the relative changes of the energy influx.

We will also be concerned with the two PN-junction detectors, oriented at $\theta = 90^{\circ}$ and $\theta = 180^{\circ}$, which were supplied by the Applied Physics Laboratory of the Johns Hopkins University. They were designed to electronically discriminate between electrons and protons, responding only to the latter, and hence may be used during the intense events to detect the presence of protons. The electronic bias for detection is given as 1.2 MeV in the most sensitive channels, 2.2, 8, and 24 MeV respectively in the higher energy channels.

III. THE ELECTRON MULTIPLIER

The electron multiplier aboard Injun III consists of a multiplier structure similar to that of a conventional photomultiplier, which is housed in an open-ended glass tube. Incident particles may strike the sensitive area of the first dynode directly and produce electrons by secondary emission. The secondaries are drawn on to successive dynodes by an accelerating potential of $\sim$130 volts/dynode. A total potential of 2500 volts applied to 19 such stages provides a current multiplication of about 2×10^5. The associated electronics contain the 2500 volt power supply and a neon-tube relaxation oscillator used as an electrometer to provide a measure of the anode current. The following discussion will consider the pertinent features of electron multiplication by secondary emission and the operation of a multiplier as a mechanical current amplifier. A description of the flight detector's constructional and operational features and the methods of calibration is included for historical purposes.

A. Electron Multipliers.

The electron multiplier structure may be considered a current amplifier providing high gain, low noise, and wide-band frequency response. Such devices have long been used to provide amplification of the feeble photoelectric currents emitted from the cathode in photomultiplier tubes, and have also been used for many years as low energy particle detectors by nuclear physicists, an effort pioneered by Allen [1947]. Because the device must be operated in a vacuum and requires no intermediate agent such as a scintillator crystal or the gas contained within the walls of a geiger counter, the multiplier serves as a true zero-wall thickness detector, responding to incident particles of sufficient energy to eject at least one secondary electron from the first dynode. The primary energy for which secondaries begin to appear is typically $\sim$20 eV [Massey and Burhop, 1952].

The electron multiplier achieves its current amplification because of secondary emission, which is the ejection of one or more electrons from a material as a result of elastic or inelastic collisions of an incident electron or ion with the surface atoms of the dynode material. The ejected electrons may be either reflected or scattered primary electrons, or true secondary electrons which are ejected from the crystal lattice of the dynode. True secondaries are emitted at low energies, generally <5 eV, which are independent of the primary particle energy. The angular distribution of the secondaries is roughly proportional to the cosine of the angle between the normal to the emitting surface and the path of the ejected secondary, and is independent of the angle of incidence of the primaries, and of the type of particle

[Bruining, 1954].

The multiplication property of a given surface is characterized by the ratio $\bar{\delta}$ of the total emitted secondary electron current to the primary electron current. This ratio is called the coefficient of secondary emission. It should be noted that this definition includes, as components of the secondary current, both elastically and inelastically scattered electrons. It should also be noted that $\bar{\delta}$ represents the average number of secondaries emitted per incident primary; in practice the value of δ associated with the incidence of any given single primary varies over a range of integral values about the mean value $\bar{\delta}$.

A comprehensive treatment of the secondary emission mechanism is given by Massey and Burhop [1952]; the properties are described in detail by these authors as well as by Bruining [1954] and Curran [1953]. Only those aspects of secondary emission that apply to the performance of an electron multiplier will be mentioned here. These aspects ultimately relate to the effect of various dynode properties on the value of $\bar{\delta}$, since it is this quantity that determines the usefulness of a given multiplier structure. For a given material the value of $\bar{\delta}$ is an extremely sensitive function of the condition of the surface of the material. $\bar{\delta}$ is also related to the energy E_p and the angle of incidence θ_p of the primary electrons, and the work function ϕ of the emitting material.

Consider now a primary electron incident on a metallic dynode. As the primary enters the target material, it loses energy rapidly due to scattering collisions. The maximum depth to which a primary penetrates will be designated d_p. True secondary electrons are generated within the material by inelastic collisions of the primary with the orbital or the free conduction electrons of the target material. The maximum depth beneath the surface of incidence from which a secondary may escape the material will be designated d_s. If the energy of the incident primary is low enough that $d_p < d_s$, $\bar{\delta}$ will increase with increasing E_p. If E_p is great enough that $d_p > d_s$, $\bar{\delta}$ will (a) continue to increase if the cross section for secondary electron production is increasing with E_p, or (b) will decrease if the cross section is decreasing with increasing E_p. The effect of E_p on $\bar{\delta}$, then, is such that $\bar{\delta}$ exhibits a maximum value at certain primary energies, usually $E_{p\ max} \sim 500$ eV, and decreases as E_p is either increased or decreased from that energy. $\bar{\delta}$ decreases rapidly for $E_p < E_{p\ max}$, but decreases quite slowly for $E_p > E_{p\ max}$.

The coefficient of secondary emission $\bar{\delta}$ is also sensitively related to the physical state of the surface of the material, since layers of contaminants on the surface as well as the crystal structure of the material result in an alteration of both d_p and d_s, principally the latter if $E_s < E_p$. Multiplier gain degradation is generally attributed to a variation of the surface properties and nature of contaminants, although it has been reported that severe vibration also adversely affects the gain [Fisher et al., 1963]. The effect of surface contaminants has been discussed by Hirashima and Miyashiro [1957], Goodrich and Wiley [1961], Treloar [1936], and Heroux and Hinteregger [1960]. It is found that, since the secondaries are emitted at such low energies, a very thin layer of foreign matter on the dynode surface is sufficient to cause appreciable decrease in $\bar{\delta}$ [Hirashima and Miyashiro, 1957]. Such surface contaminants may be due to (a) deposition of insulating layers of carbonaceous matter due to the presence of hydrocarbon vapors within the vacuum system in which the multiplier <u>must</u> be used, (b) the adsorption of a monolayer of atmospheric gases on the dynode, and (c) the production of oxides or hydroxides due to exposure of the dynode surfaces to the atmosphere. Great care must be exercised when handling electron multiplier structures to insure that these factors affecting $\bar{\delta}$ are controlled as well as possible. Later sections will deal in more detail with the observed effects and methods of handling the multiplier structure.

B. The Injun III Electron Multiplier.

One of the low energy electron detectors launched with Injun III utilizes a conventional multiplier structure similar to those employed in the Injun III photometers and the DC scintillator.

The unit was obtained with the flat face and photocathode removed and a glass break-away cap in their place. After removal of this cap, the aperture assembly containing a spring loaded trap-door mechanism provides an "O" ring seal so that the structure may be contained in an inert atmosphere of dry N_2 at a few millimeters of pressure to minimize dynode deterioration. The spring loading was sufficient to insure the opening of the door after launch when the pressure of the earth's atmosphere was no longer present, thus exposing the first dynode to incident particles of sufficient energy to penetrate the foil-covered opening. The multiplier thus serves as a current amplifier, responding with nearly constant efficiency to electrons of energy $10 \leq E_e \leq 100$ keV. The anode current from the multiplier is proportional to the incident particle number flux.

Analog to digital conversion of the anode current is accomplished by a simple neon-glow tube relaxation oscillator whose output frequency is a function of the current drawn from the circuit input. High voltage was supplied to the dynodes by a regulated 2500 volt supply. Since the anode was referenced to ground potential, the voltage applied to the first dynode was -2500 volts.

The multiplier structure itself was a 19 stage venetian blind structure patterned after those used in the Ascop 541 series photomultiplier tubes, manufactured by Electro-Mechanical Research, Inc., Princeton, New Jersey. The dynode material was Ag(MgO) with no alkali metal activation such as usually found in photomultiplier structures of this type. The first dynode had an active area of $.15\ cm^2$, and the separation between adjacent dynodes is $\sim .25$ cm. With 2500 volts applied to the dynode voltage divider resistors, which are mounted in the tube itself and potted in Silastic rubber, the interstage accelerating potential is 130 volts/stage. The minimal design gain of the tube was to be $\approx 5 \times 10^6$ at this applied voltage.

The venetian blind structure is an appropriate structure for this application for two reasons. First, the venetian blind structure generally (and particularly of this manufacturer) is the most rugged, thus enabling the tube to withstand the vibration encountered during launch. Secondly, the electron optics of such a structure are by far the least critical. Since the multiplier was located near the alignment magnets of Injun III, thus in an ambient field of .7 gauss aligned at approximately 90^o to the longitudinal axis of the tube, possible degradation of gain due to a defocussing effect of the field was minimized by choosing a structure of the venetian blind type.

It was also necessary that the dynode material be able to withstand limited exposure to the atmosphere with little degradation of the multiplier gain, but that a material with a high $\bar{\delta}$ be used to provide as high a gain as possible.

The dynodes could have been of two possible materials: copper-beryllium or silver-magnesium. All other materials in common use employ antimony or cesium activating layers, which are extremely sensitive to atmospheric contamination. On the basis of discussions with several workers in the field of low energy particle detection with electron multipliers, it was felt that Ag(MgO) could offer a somewhat higher value of $\bar{\delta}$ than copper-beryllium, but that the resistance of this material to atmospheric contaminants was somewhat less than that of copper-beryllium. On the basis that it would be easier to develop methods by which the tube could be protected from exposure to the atmosphere than it would be to increase the applied tube voltage above the 2500 volt nominal, or to add additional dynode stages to a copper-beryllium structure, it was decided that Ag(MgO) would offer the best combination of high gain with reasonable resistance to gain degradation.

The multipliers were handled at all times in such a way as to minimize exposure to the atmosphere. The tubes were shipped under vacuum in a sealed glass housing with a break-away cap which was grooved for scoring with a diamond pencil. The caps were removed using the hot wire technique. This operation was performed in a dry box filled with dry N_2. Upon opening, the tubes were immediately assembled into the housing and electronics. Complete electrical testing of the module had already been completed, as will be discussed later. It is estimated that during the portion of the lifetime of the tube after the initial pumpdown and bake-out,* total duration of exposure to the ambient atmosphere was less than 40 minutes. All operations requiring access to the open structure during the final preparation and calibration of the flight units were performed in the dry box.

The multiplier structure was mounted in a magnesium housing and was shielded with 0.25 mm of lead, 0.15 mm "Netic" magnetic shielding (density ~ 7.7 g/cm^3), and minimally 4.5 mm of magnesium. The complete assembly is shown in Figure 2.

The trap-door assembly, containing the entrance collimator, provided air-tight seals so that after calibration and during storage and transit prior to launch the multiplier could be stored in an inert atmosphere of N_2. In addition to the trap door, an outer safety cap also seated against an "O" ring provided an additional volume filled with dry N_2 around the exterior of the

---

* The manufacturer maintained a vacuum of at least 10^{-7} mm Hg while the multiplier structure was baked at 400°C for four hours. After completion of bakeout, evacuation was continued for another 24 hours, whereupon the tube was sealed [Yingling, private communication].

trap door. This was for additional backup protection to insure that, should the trap-door seal leak, only N_2 would be allowed into the tube. The measured leak rate in one atmosphere of the trap-door assembly mounted on a container of similar volume indicated the initial pressure increase within the volume to be about .4 mm Hg/day. The spring-loaded trap door utilized the pressure differential between the inside and outside of the volume to keep the door closed. It was established experimentally that if the pressure inside the container were as high as 50 mm the door would spring open. On the basis of the measured leak rate given above, and assuming it to be uniform throughout the range of internal pressures from 0 - 50 mm, the useful shelf life of the unit, before the door would open, was estimated to be 100 days, or about three months.

The defining aperture and collimating piece were of 15% leaded-nickel-silver (density = 8.2 g/cm^3). The rear aperture was covered by a 86 $\mu g/cm^2$ (1000Å) nickel foil which served two purposes. First, the foil attenuated incident light striking the sensitive surfaces, thus minimizing false signal due to the sun's ultra-violet and visible radiation. Other sources of light encountered in orbit produce negligible effects. Secondly, because such a foil was an absolute necessity to protect the companion detector to the electron multiplier, the DC scintillator, from damage due to sunlight, it was deemed desirable to employ a similar foil, thus imposing a comparable low energy threshold on the two units. The foil used imposes a threshold of 9 keV for direct penetration by electrons. This energy corresponds to that required by an electron of an altitude of $\sim$ 1000 km to penetrate the atmosphere to an auroral altitude of $\sim$100 km.

The electronics consisted of two units, a 2500 volt supply and an integrating electrometer circuit. These are shown schematically in Figure 3. The anode current was converted to digital form for transmission via the telemetry link by a neon relaxation oscillator similar to that described previously by Freeman [1961]. The present circuit is different only in that it employed a locally generated sawtooth waveform injected on the low side of the integrating capacitor. This waveform, $\sim$4 volts peak-to-peak in amplitude and at a frequency of $\sim$200 cps, serves as a "tickle" voltage to be applied to the neon tube. It has been noticed that, at certain input currents, the neon tube may well go into a state of partial conduction as the potential difference across the capacitor nears the firing voltage. This allows a small but continuous current to flow, which is sufficient to prevent the capacitor from attaining enough charge to produce full firing voltage across the tube. For such a state of partial conduction there appears to be no corresponding extinction potential, for the tube will maintain this quiescent conduction as the input current is decreased. The application of the tickle voltage is to supply a small step function in the integration waveform to insure that the neon tube is driven into full conduction.

C. Testing and Calibration.

Complete electrical testing and calibrations were completed prior to the installation of the trap-door assembly, i.e., before the glass break-away cap was removed. This was to insure that no electronic failures were likely to occur which would require additional disassembly and reassembly of the unit, thereby risking degradation of the multiplier gain. These calibrations and tests will be referred to as the preassembly calibration procedure. The glass cap was then removed, the unit assembled, and calibrated as a particle detector with an electron gun and a Po^{210} alpha source.

During the preassembly calibration, particle input was simulated by illuminating the multiplier structure through the glass cap with a small incandescent bulb. The bulb was mounted in a fixture to insure that the lamp-to-dynode distance would remain constant, and to provide an easy means of interposing Kodak neutral density filters to vary the light intensity by a known and reproducible amount. This fixture will be referred to as the "lamp holder" fixture. The anode terminal was readily available so that the absolute current output of the multiplier could be measured by a commercial electrometer while the tube was operated from the flight power supply. In this way, frequent verification that the neon tube electrometer circuit was operating properly was possible.

The preassembly calibrations included the following tests:

1. The current-to-frequency conversion properties of the electrometer were obtained directly by recording the measured current output of the tube and the corresponding frequency output of the neon tube electrometer due to a known input illumination. The linearity of response of both the multiplier tube alone and the multiplier-electrometer combined were determined in this way. These are shown in Figure 4. These properties were verified at temperature intervals of 15° between $-20^{\circ}C$ and $55^{\circ}C$; variations over this range were found to be less than 10%. Dark current throughout this range of temperatures was measured and found to be less than 10^{-11} ampere.
2. Output voltage and current of the high voltage supply over the same range of temperatures and over the range of input voltage from 18 to 26 volts were also determined. It was found that these

environmental factors produced negligible effects on the above parameters. The unit underwent seven complete temperature and voltage cycles during the course of these tests. The power supply properties were monitored during all seven cycles, the neon-tube electrometer was checked on three cycles.

Calibration of the detector for electrons was accomplished by an electron gun capable of producing monoenergetic electrons over the range from 2 to 100 keV. This gun is similar to the type described by Frank [1959] and by Freeman [1961]. The detector was mounted adjacent to a Faraday cup on a movable jig. Either the detector or the cup could be placed in a given position near the center of the electron beam. The cup was provided to monitor the beam current; the bottom and edges were beveled on the interior and coated with Aquadag to minimize secondary electron emission. The detector could be rotated about an axis perpendicular to the beam to determine the sensitivity to obliquely incident electrons.

The absolute response of the detector to electron fluxes is shown in Figure 5. The unit of flux is electrons (cm^2 second steradian)$^{-1}$. It will be noticed that above 15 keV the detector response is essentially independent of electron energy. The decreasing sensitivity below this point is due to (a) the presence of the foil, and (b) the presence of the -2500 volt potential on the first dynode. The effect of these is shown in Figure 6. Curve A shows the relative response of the flight detector with the foil in place and the first dynode at -2500 volts. Curve B illustrates the effect of the retarding potential on the response of the detector with the same foil, but with the first dynode at ground potential. Curve C illustrates the effect of the foil alone on the response of a similar detector. The first dynode of this detector is at -2500 volts, but the foil is omitted.

The gain of the multiplier can be calculated from knowledge of the beam current density as measured by the Faraday cup and the area of the defining aperture of the detector. The current gain thus determined was 2.5×10^5, as opposed to the manufacturer's stated design goal of 5×10^6. The discrepancy is thought to be the result of an adsorbed monolayer of atmospheric gases on the dynode surfaces. It was impossible, however, to verify this speculation because the high temperature bakeout required to remove such a layer, if present, would damage the dynode voltage divider resistors as well as the Silastic rubber potting around the tube. Support of this supposition is offered by the observations of Hirashima and Miyashiro [1957] which will be discussed later.

The angular resolution of the flight unit was determined by rotating the detector axis with respect to the incident electron beam. This was done at beam energies of 15, 30, 50, and 90 keV for a variety of collimation configurations and alternate collimator materials of leaded-nickel-silver and stainless steel. Changing the collimator material appeared to affect the shape of these curves somewhat more than a change of the collimator geometry; neither effect is considered significant.

The relative sensitivity $f_E(\Theta)$ of the multiplier to electrons of energy E incident at an angle Θ to the collimator axis is shown in Figure 7. The response at $\Theta = 0^o$ was normalized to unit relative sensitivity for each energy E. The directional geometric factor g of the detector was calculated using the function $f_E(\Theta)$ and the relation

$$g = \frac{1}{2\pi} \int_0^{2\pi} \int_0^{\pi/2} a\, f(\Theta) \cos \Theta \, d\,\Theta \, d\,\phi$$

where a is the area of the front aperture. Rotational symmetry about the polar angle ϕ, i.e., about the collimator axis, is assumed. The value of g thus determined is 1.2×10^{-2} cm^2 sterad.

Response of the instrument to a Po^{210} alpha source of $\sim$1 mc activity was determined in vacuo. It was found that a flux incident on the first dynode, and estimated to be $\sim 10^5$ particles/second of energy $E_\alpha > 420$ keV [Fillius, private communication] produced an output rate of .6 cps from the electrometer. The response of the detector per incident α particle is thus seen to be about twice to four times the response per incident electron.

The effects of exposure of a similar dynode structure to dry O_2 and N_2 at a pressure of one atmosphere were determined with a Ni^{62} beta source. The source and detector were fixed relative to one another within a vacuum chanber. Response of the detector to the source was determined after each of four successive seven-hour periods of exposure to O_2. The gain improved very slightly ($\sim 5\%$) after three such periods, but remained constant after the last storage period. The response of this tube after a storage period of nine days in dry N_2 produced no observable change in the detector sensitivity. The multiplier was handled throughout this procedure in an identical manner as the flight tube.

The means by which the multiplier performance may progressively deteriorate is due to (a) degradation of the gain by atmospheric contamination of the dynode surfaces, or (b) deposition on the dynode of an insulating layer of material having an inferior secondary electron yield. Hirashima and Miyashiro [1957] have reported on these affects with specific reference to AgMg dynodes. Much of the following is based on this report.

Degradation of the multiplier gain by atmospheric contamination may be due to either physical or chemical action of the atmospheric constituents on the dynode surfaces. The physical adherence of an adsorbed monolayer of atmospheric gases on the dynode surface has been observed by Hirashima and Miyashiro to constitute a principal cause of decay of $\bar{\delta}$. The gain may be subsequently restored after a thorough out-gassing procedure. Chemical action of the atmosphere on the dynodes is usually attributed to the formation of oxides or hydroxides. The resulting yield decay is generally quite severe, but the time required for such action to occur is on the order of an hour or more. It is reported that AgMg dynodes activated by exposure to oxygen for a few minutes at a temperature of 600°C evidenced no change of $\bar{\delta}$ due to a subsequent "short-term" exposure to air at a temperature of 590°C.

Support of the previous speculation that the observed discrepancy of the measured multiplier gain and that predicted by the manufacturer may be due to adsorbed gases is offered by consideration of the following observation in the light of the reports cited above. It was noted that the flight tube evidenced no progressive change of gain after each of three successive exposures to the atmosphere. Each exposure is estimated to be $\sim$10 minutes. If the presumed degradation is assumed to be due to a chemical process initiated by the presence of air, it must therefore be a process that essentially "goes to completion" during the first 10-minute exposure to the atmosphere at a temperature of $\sim 30^{\circ}$C. On the basis of these observations and those of Hirashima and Miyashiro, it appears likely that adsorbed layers of atmospheric gases, not chemical action, is responsible for the presumed decay.

With regard to degradation of multiplier gain due to the deposition of insulating layers on the dynode surfaces, the following remarks are in order. It has been reported [Hirashima and Miyashiro, 1957] that a decrease in $\bar{\delta}$ accompanies the bombardment of Ag(MgO) in vacuo by an electron beam of current density ~ 1 to 3×10^{-7} amp/cm^2. The degree of degradation is roughly proportional to the integrated charge delivered to the sample. On the basis of electron diffraction studies of a dynode surface subjected to electron bombardment, it was concluded that the contaminant was "amorphous and carbonaceous." Since hydrocarbon molecules are known to be present within vacuum systems using oil diffusion pumps, and are known to decompose with electron bombardment, Hirashima and Miyashiro concluded that deterioration of $\bar{\delta}$ could be minimized either by avoiding beam current densities greater than $\sim 10^{-7}$ amp/cm^2, or by using a vacuum system in which hydrocarbon molecules were not present. The latter conclusion was tested by replacing the oil pump with a mercury diffusion pump. The observed decay of $\bar{\delta}$ was indeed observed to be substantially less severe when the mercury diffusion pump was used.

During all calibrations, care was exercised to insure that the anode current did not exceed 1×10^{-7} amp (corresponding to a current density at the anode of 3×10^{-7} amp/cm^2). Previous tubes that had been subjected to higher beam currents did indeed show a rapid gain decrease at anode currents greater than $\sim 8 \times 10^{-7}$ amp. On the basis of this observation and the results of Hirashima and Miyashiro, and since no such progressive gain decrease was noticed throughout the calibration procedure, it is felt that no significant damage to the dynode surfaces resulted from either atmospheric contamination or from the deposition of materials of low secondary yield.

D. <u>Post-Launch Calibration Checks</u>.

Proper operation of the multiplier after launch with respect to survival of the foil and degradation of gain was investigated. The method and conclusions will be given here.

Presence of the foil may be verified by noting the response of the detector to sunlight. Times for which the sun was within the viewing cone of the detector may be determined by the optical aspect sensor and the DC scintillator. Checks performed at various times in the post-launch career of the satellite indicate that the foil is substantially intact within the limits set by our knowledge of the detector response to light. Prior to the removal of the glass cap, it was observed that a 12 watt incandescent bulb was sufficient to produce an anode current of $\sim 10^{-5}$ amp. After installation of the foil and aperture assembly, a 500 watt projection lamp illuminating the entrance aperture from a distance of 22 inches produced an anode current less than 10^{-10} amp. Response of the multiplier after launch to direct sunlight has been observed consistently to be less than $\sim 3 \times 10^{-2}$ cps, equivalent to an anode current of 2×10^{-10} amp.

Evidence that the multiplier gain has not progressively decreased since launch is offered by noting the response of the tube to sunlight periodically during the operational lifetime. This has been done for 11 occasions, the most recent being on 25 June 1963. No significant change of response from that initially observed has been noted. It is therefore suggested that the tube gain has remained constant within $\sim 10\%$ over the six-month period.

Survival of the multiplier gain in the period between the time of prelaunch calibration and the time of launch is indicated by the fact that at no time has the multiplier response been less than that to be expected due to a known particle flux as indicated by the geiger tubes. However, the multiplier is sensitive only to such large fluxes that the geiger tubes are driven into the non-linear regions of their response curves at those times when comparisons may be made. The uncertainties associated with the non-linear regions of the geiger tubes warrant comment.

In-flight checks of the geiger tubes have revealed somewhat higher apparent rates than the observed preflight maxima. Since the slope of the response curve of a geiger tube approaches zero near the maximum apparent rate, determination of the true rate is subject to error. A revised curve was fitted between the linear region and the new maximum rate as a first approximation to recalibration. An indication of the probable validity of this procedure is possible by comparing the predicted true rate thus obtained with that of another detector operating in its linear range. The only such detector is the differential spectrometer, which is generally not saturated by virtue of its small geometric factor; this is parallel to only one of the three discrepant geigers. Justification that this detector can thus be used rests on the following argument.

The slope of the spectrum in the energy range 40 to 100 keV can be determined by the ratio SpL/SpH. Assuming an exponential representation of the spectrum as

$$N(E)dE = N_o e^{-E/E_o}\, dE$$

we determine E_o from SpL/SpH, and N_o from the expression

$$SpL = \int_o^{\infty} \epsilon\, g(E) N_o e^{-E/E_o}\, dE$$

The function ϵ g(E) is determined experimentally and may be thought of as the passband of the low energy channel. The integration is carried out numerically. Once N_o is obtained, we determine the integral flux $J(>E)$ directly. The flux thus predicted is accurate within the limitations imposed by the assumption that the spectral model properly represents the flux present. Verification that this discrepancy is small indeed is provided by a measurement of the real flux $J(E_e > 250\ \text{keV})$ obtained from 213B and $J(E_e > 1.3\ \text{MeV})$ obtained from IsL. The spectrum does not continue to decrease as predicted by the exponential form, but the integral flux $J(E_e > 250\ \text{keV})$ determined by 213B is less than 1% of the flux $J(E_e > 40\ \text{keV})$. It is thus claimed that the true flux at pitch angles $\alpha = 90^{\circ}$ may be determined with SpL and SpH with an accuracy of about 50%.

We may now test the accuracy of the revised response curve of 213A by comparing our predicted flux $J(E_e > 40\ \text{keV})$ derived from spectrometer data with the actual flux determined from 213A. This has been done for some 50 cases, for which it was found that the disagreement was always less than about 50%, and that these disagreements were approximately equally distributed in sign. This may be interpreted as indicating no systematic error is present in the above approach.

To extend the same argument to a verification of a similarly revised response curve for the 213C, we must assume that both the flux and the spectral shape are essentially constant over pitch angles from 87° to 145°. If this is so, we are allowed the use of the spectrometer to predict the absolute flux at 130°.

Let it initially be assumed that the flux during intense events is truly isotropic. Then a comparison of the flux present as determined by 213C and SpL again indicates quite close agreement, with only a slightly greater probability (.6) for J_{213C} to be greater than J_{213A}.

The validity with which it may be claimed that the flux may be considered isotropic is thus crucial in substantiating the proposed revision of the thin-windowed geiger tubes at $\Theta = 90^{\circ}$ and $\Theta = 130^{\circ}$. We discuss here the basis of this assumption. O'Brien [1962 a and b] has shown that the angular distribution of particles measured by Injun I definitely approaches isotropy well within a factor of 2 within the range of L and α considered in this study. Some preliminary studies with Injun III to investigate the isotropy of fluxes during less intense, but nevertheless disturbed events, also indicate the assumption of isotropy is well founded [O'Brien, private communication].

IV. PROCEDURE

The intent of this investigation is to describe some of the features of the high latitude intense events observed by Injun III with particular interest in the behavior of the low energy component of the corpuscular radiation present. Those detectors which will be of use in this endeavor have been described in a previous section. It is desirable at this point to review very briefly what is known of the general character of the outer zone during both quiet and disturbed times and to discuss the few reported investigations of low energy particle radiation in the outer zone. The manner in which the detector complement of Injun III will be used to determine the parameters of significance in this investigation will also be discussed.

A. The Outer Zone.

The rather chaotic state of knowledge regarding the outer zone has been remedied only in the past year with the publication of the results of several definitive measurements of the absolute particle flux and energy spectrum within the outer zone. The history of controversy of outer-zone investigations has recently been summarized by O'Brien [1963a] and by Farley [1963]. These serve extremely well as a brief review of experimental data and to chronicle the course of past experimentation. What follows is to serve only as a brief report of recent measurements of the particle flux and energy spectrum in the outer zone.

The particle types found in the outer zone are principally protons and electrons, with less than 1% of the flux due to heavier particles. The proton and electron components are thought to be equal in number [Farley, 1963] but the dominant particles of penetrating energies are known to be electrons. During undisturbed periods the angular distribution of both particle types is generally peaked at 90° to the field line [O'Brien, 1963].

One report of the low energy ($E_p \leq 1$ MeV) proton component in the outer zone is that of Davis and Williamson [1962], who have obtained from scintillators on Explorer XII a measure of the proton energy spectra in the range 100 keV $\leq E_p \leq 4.5$ MeV. In the heart of the outer zone, at L = 3 to 5, a very broad maximum of directional particle flux $j(E_p > 100 \text{ keV}) \sim 7 \times 10^6/\text{cm}^2$ sec sterad was observed during a single pass. The flux throughout $2 \leq L \leq 8$ was comparable within a factor of 5. The energy spectrum is reported to be of the exponential form

$$j(E)dE = N_o e^{-E/E_o} dE$$

in which E_o = 400 keV at L = 2.85 and E_o = 64 keV at L = 6.1. The equatorial angular distribution $j_o(\alpha_o)$ of these particles was reported to be proportional to $\sin^3 \alpha_o$ in the range of α_o from 10° to 70°.

Frank et al. [1963] report the proton flux to be $J(E_p > 500$ keV) $\sim 4 \times 10^6/\mathrm{cm}^2$ sec at $L \sim 6$ and near the equatorial plane.

Proton outfluxes from the outer zone have been observed by McIlwain [1959] to be $j(E_p > 70$ keV) $= 3 \times 10^5/\mathrm{cm}^2$ sec sterad within a visible auroral arc at an altitude of 120 km. These protons exhibited an energy spectrum of the above form in which $E_o = 30$ keV. On the basis of this spectrum, assuming it to be valid to $E = 0$, the proton flux incident on the top of the atmosphere is estimated to be $1.6 \times 10^7/\mathrm{cm}^2$ sec.

Reports of measurements by many investigators of the electron content within the outer zone are somewhat more numerous in the literature. Recent observations in the region of $L > 2$ near the equatorial plane have shown the intensity $J(E_e > 40$ keV) to be $\approx 10^7/\mathrm{cm}^2$ sec within an order of magnitude throughout the entire region. These observations thus show little of the "classical" zone-like structure with a distinct slot at the lower edge [Rosser et al., 1962 and O'Brien et al., 1962b]. Measurements with similar detectors at these L values but at magnetic latitudes $\lambda_m \gtrsim 45^\circ$ indicate the average electron flux $j(E_e > 40$ keV) is typically $10^5/\mathrm{cm}^2$ sec sterad and is variable with time by at least an order of magnitude at any given L value [O'Brien, 1962a].

The higher energy electrons ($E_e > 1.6$ MeV) are found [Freeman, 1963] in intensities $J(E_e \gtrsim 1.6$ MeV) $\approx 4 \times 10^3/\mathrm{cm}^2$ sec at low latitudes in the outer zone ($L \sim 3$). At higher latitudes, but similar L values, this electron flux is quite similar, generally $\sim 10^3$ [Forbush et al., 1962]. That the classical zonal structure is preserved at these energies is demonstrated by comparing the above fluxes with similar measurements at higher L values, also given by Freeman [1963]. These are $J(E_e \geq 1.6 \text{ MeV}) \approx 4 \times 10^1/\text{cm}^2$ sec at $L = 7.5$ near the equatorial plane and, at higher latitudes, $J(E_e \geq 1.6 \text{ MeV}) \approx 10^1/\text{cm}^2$ sec at $L = 7.5$ and 700 km altitude [Fritz, private communication]. These observations indicate that the omnidirectional flux varies distinctly as a function of L.

The energy spectrum of the outer zone electrons during "typical quiet times" is reported by Freeman [1963] to be of the form

$$N(E)dE = KE^{-\gamma}dE$$

and is characterized by values of $\gamma = 0$ at $L = 3$ and $\gamma = 3.5$ at $L \sim 10$ near the geomagnetic equator. Corresponding values of γ on these L shells, but at 1000 km altitude, derived from work of O'Brien et al. [1962a] are given as $\gamma = 0$ to 1 at $L = 3$, and $\gamma = 3$ to 5 at $L = 7.5$.

It should be emphasized that both the intensity and spectral characteristics of these outer-zone electrons are variable with time even during magnetically "quiet" periods. Order-of-magnitude changes the intensity $J(E_e > 40$ keV) are apparent in intervals as short as a few seconds or distances of a few kilometers, while changes of the electron flux $J(E_e > 1.6$ MeV) have been observed to be as great as two or more orders of magnitude in a period of hours [O'Brien, 1963a and Freeman, 1963]. Spectral variations are similarly extreme, as one would expect because of the relatively unrelated variability of the high and low energy electron fluxes noted. The spectral characteristics given above may be regarded as typical, but individual values of γ might well vary by as much as a factor of two. It is certain, however, that the electron spectrum is generally softer at greater L values both near the equatorial plane as well as at high latitudes and 1000 km altitudes. This general spectral pattern thus appears to be consistent throughout the entire outer zone.

The generalized storm-time features of the outer zone evident during periods of magnetic disturbance have recently been reported by Freeman [1963] and Rosser [1963] based on observations with Explorer XII. Earlier reports due to Forbush et al. [1962] and Rothwell and McIlwain [1959] are based on similar studies with Explorers VII and IV respectively. Briefly, the features reported by Freeman, based on an analysis of several disturbances, indicate that (a) the low energy electron ($E_e \lesssim 100$ keV) content increases throughout the zone with increasing level of magnetic activity and evidences rapid temporal and/or spatial variations, and (b) the high energy electron component ($E_e \gtrsim 1.6$ MeV) is diminished during the initial and early storm phase, but is enhanced well above the quiescent level during the late recovery phase in the region of $L = 3.5$ to $L = 5$, with greater enhancements appearing at larger L values. The high energy component does not display the increased temporal or spatial variability. Other reports referenced above depict a similar generalized morphology of the outer zone during periods of magnetic disturbance and need not be reviewed here. The salient features are well reported by Freeman.

B. Very Low Energy Particles.

Detection of very low energy ($1 \text{ keV} \leq E_e \leq 40$ keV) electrons within the outer zone has been reported by Krasovskii et al. [1961]. Omnidirectional electron fluxes on the order of $J(E_e > 10 \text{ keV}) \sim 10^9/\text{cm}^2$ sec or greater were observed on one pass at 1800 $\pm$ 100 km altitude at $\sim 50^\circ$ South geographic latitude ($\sim -60^\circ$ geomagnetic latitude) over the South Pacific. The observed responses of the shielded and unshielded scintillators were compatible with a mono-energetic electron beam of $E_e = 14$ keV. Also within the outer zone, observations by O'Brien and Laughlin [1962] utilizing the total energy detector on Injun I indicate fluxes of $j(E_e \gtrsim 10 \text{ keV}) \sim 10^{10}/\text{cm}^2$ sec sterad at $L \sim 8$ to 10 and at $\lambda_m \sim 60^\circ$ during a single intense event. Measurements with Lunik 2 [Gringauz et al., 1961] indicate the intensity of low energy fluxes $J(E_e \geq 200 \text{ eV}) \sim 10^8/\text{cm}^2$ sec at great radial distances ($L \sim 10$) and near the equatorial plane, Hoffman et al. [1962] have observed on one occasion a peak electron flux $j(10 \leq E_e \leq 35 \text{ keV}) \sim 3 \times 10^6/\text{cm}^2$ sec sterad immediately preceding a geomagnetic storm.

Direct observations by rocket-borne apparatus of outfluxes of very low energy electrons from the outer zone have been reported by McIlwain [1959], Davis et al. [1960], and McDiarmid et al. [1961]. These fluxes were all declared to be associated with auroral phenomena. McIlwain detected, at ~ 120 km and within visible aurora, fluxes of $j(E_e \gtrsim 3 \text{ keV}) \approx 2 \times 10^9/\text{cm}^2$ sec sterad and $2 \times 10^{11}/\text{cm}^2$ sec sterad on two separate flights. The spectral characteristics of the first observation could be characterized by an exponential function of the nature reported earlier in which the shape parameter $E_o = 5$ keV. The second flight detected an electron flux that appeared to be monoenergetic at an energy of ~ 6 keV. Davis et al. report fluxes $j(E_e > 8 \text{ keV}) \approx 2 - 6 \times 10^7/\text{cm}^2$ sec sterad with a somewhat harder spectrum. A five-electrode "electron trap" sensitive to electrons of energy $30 \text{ eV} \leq E_e \leq 1$ keV indicated a total flux $\lesssim 10^9/\text{cm}^2$ sec sterad. McDiarmid et al. observed similar fluxes of higher energy particles of $J(E_e \gtrsim 30 \text{ keV}) \sim 2 \times 10^6$ following an exponential spectral distribution in which $E_o = 22$ keV. All these reports indicate that large and rapid variations of intensity are apparent during the minutes-long rocket flight. However, no similar observations of the spectral behavior with time or intensity are reported.

In the presentation of the following observations of intense events, the features that will be considered are (a) the electron energy spectrum in the range 10 keV $\leq E_e \leq$ 1 MeV and its temporal/spatial variations, and (b) the observed variations of the particle flux with pitch angle, with time, and with L. Since the events are observed for such a short period of time (typically $\sim$2 minutes), any dependence on $\underline{B}$ is difficult to ascertain because the range of $\underline{B}$ traversed is quite small. The typical variation of $\underline{B}$ during an observation is from .41 to .44 gauss. We will instead consider altitude a parameter of possible interest.

Additional features of interest are the presence of VLF and/or auroral light emissions associated with the events to be discussed. Such phenomenon will be reported in a qualitative manner; extensive investigations are being conducted by Gurnett [1963] and Taylor [private communication]. The nature of these phenomena as presented here will be due to the above cited sources. Such reports are intended only to illustrate the association observed between particle, auroral, and VLF observations during these events. An investigation to consider the details of the interrelations is planned.

The instrumental complement of Injun III enables determination of a six point energy spectrum of trapped electrons with points at 40, 100, and 250 keV and 1.3, 3, and 5 MeV. Rudimentary determination of the energy spectrum at $\alpha = 50^\circ$ when the particle intensity is sufficiently great $J(E_e \gtrsim 10 \text{ keV}) \sim 10^6/\text{cm}^2$ sec sterad is possible with points at 10 and 40 keV. The assumption of isotropy of spectra at $\alpha = 90^\circ$ and $\alpha = 50^\circ$ allows the extension of the above spectra to include the point at 10 keV. The instantaneous angular distribution of electrons of $E_e \gtrsim 40$ keV about the local $\underline{B}$ vector may be determined with the geiger tubes 213A, C, D, and the differential spectrometer, which are oriented at $\theta = 90^\circ$, 130°, 180°, and 270° respectively to the alignment axis of the satellite. The method of analysis of these features is given here.

1. Energy Spectra.

Previous reports of the energy spectra in the outer zone have generally been represented either by an exponential function of the form

$$N(E)dE = N_o e^{-E/E_o} dE$$

or a power-law function such as

$$N(E)dE = KE^{-\gamma} dE$$

The quantities E_o and γ may be termed the shape parameter in these expressions in that the numerical value of these quantities completely determines the differential properties of the spectral representation. Since both spectral forms contain two adjustable parameters, two independent measurements of the particle flux in different energy ranges are required to assign numerical values to the quantities of either expression. In the following, two such determinations are possible, one based on SpL and SpH, the second based on EM and SpL.

Consider first the evaluation of both adjustable parameters of a given spectral model on the basis of SpL and SpH. The method [Laughlin, private communication] by which this was done initially assumed a spectral form in which the shape parameter E_o or γ was given numerical values and the expected response of both SpL and SpH calculated using

$$D_i = \int_o^{\infty} R_i(E)N(E)dE$$

where

D_i = response of either SpL or SpH in cps.

$R_i(E)$ = the response function of the detector derived from preflight calibrations in units of cps (particles/cm^2 sec sterad)$^{-1}$.

$N(E)dE$ = the spectral model assumed.

Note that D_i is the designation of the i^{th} detector as given in

Table I and may be used to refer to either the detector itself or the response (in cps) of that detector depending on the context of its usage. For the differential spectrometer channels, $R_i(E)$ is given as $g_i(E)$ and may be considered as the passband of the detector. The quantity also includes detector efficiency and the geometric factors. The ratio SpL/SpH is thus given by

$$\frac{SpL}{SpH} = \frac{\int_0^{\infty} R_{SpL}(E)N(E)dE}{\int_0^{\infty} R_{SpH}(E)N(E)dE}$$

and is independent of N_o or K in the two spectral models used. The integrations are carried out numerically and the results for various values of E_o and γ in the respective spectral forms are tabulated. The ratio is thus calculated and graphed as a function of E_o or γ. This graph then serves as a tool by which the value of the shape parameter representing an observed SpL/SpH may be easily determined. A family of curves representing SpL, the count rate of the low channel, as a function of either N_o or K for given values of E_o or γ respectively, permits rapid determination of the proper N_o or K. This completes the numeric expression by which a given observation may be represented. Such a determination is limited in accuracy to the expression of the differential distribution of electrons in the range of energies from 40 to 100 keV, and is predicated on the assumption of a given spectral model.

Determination of shape parameter of these spectral models on the basis of EM and SpL is accomplished by first evaluating the observed flux intensities $J(> 10 \text{ keV})$ and $J(> 40 \text{ keV})$ from the detector calibrations. The method by which $J(> 10 \text{ keV})$ and $J(> 40 \text{ keV})$ may be determined with these detectors has been discussed in an earlier chapter. The ratio $J(> 10 \text{ keV}) / J(> 40 \text{ keV})$ is calculated for assigned values of E_o or γ and plotted as a function of these variables. Such a plot thus serves as a useful tool by which E_o or γ may be conveniently evaluated for a given pair of observations. The numerical value of the shape parameter thus determined is predicated on the assumption of a given spectral model, and is applicable in the range of energy $10 \text{ keV} \leq E_e \leq 40 \text{ keV}$. Parenthetically, it should be noted that the original intention was to employ DC for this purpose. It is anticipated that a re-evaluation of the gain of DC, which is currently in progress, will permit this intention to be fulfilled.

In practice, it has been found that observations cannot be accurately represented by either such model, but that the exponential is more often useful and provides a reasonable fit to the observations at the 10, 40, and 90 keV points. For this reason, the observations are reported with reference to the exponential expression to facilitate comparison of these observations with the results of previous experimentation.

Since the count rate of EM is generally quite low, $\sim 10^{-1}$ count/frame, the determination of $J(>10\text{ keV})$ thus represents a time average of the flux over an interval of several seconds. It is therefore necessary that the corresponding flux $J(>40\text{ keV})$ also be averaged over the same interval. However, the intensity of the events to be studied is sufficient to drive the thin-windowed geiger tubes into the non-linear region of their response curves. It is therefore of importance to emphasize that the average flux $J(>40\text{ keV})$ utilized in the spectral determinations to follow was derived from the averaged true count rate of 213C, not the averaged apparent count rate. The accuracy of $J(>40\text{ keV})$ shown in the spectra to be presented is felt to be accurate within a factor of two when all sources of error are considered. The principal source of error has been discussed in a previous chapter.

The determination of $J(>10\text{ keV})$ is plotted in the spectra to follow with a somewhat larger error bar. These limits were determined by assuming the incident flux to be monoenergetic at those values of E_e where (a) $R_{EM}(E)$ is a maximum, i.e., $E_e \approx 60$ keV, and (b) $R_{EM}(E)$ is attenuated by a factor of 4, i.e., $E_e \approx 10$ keV. Since the gain of the multiplier could possibly decrease, but could never increase, it is therefore felt that the lower end of the error bar on the values $j(E_e \leq 10\text{ keV})$ represents an absolute lower limit of the determination of the flux of electrons of energy $E_e \gtrsim 10$ keV.

2. Angular Distribution.

The matter of specifying the angular distribution $j(\alpha)$ of the observed radiation in terms of a model function, as was discussed above with reference to the spectral distribution, is not of import to the present investigation. The events to be studied do evidence some extremely interesting features that require a brief discussion of the method of observing the angular distribution, at least in a qualitative manner. The thin-windowed geiger counters 213A, C, and D, oriented at 90°, 130°, and 180° respectively, may be used to determine the average directional flux at pitch angles of $\alpha = 90^\circ \pm \sim 10^\circ$, $50^\circ \pm \sim 10^\circ$, and $0^\circ \pm \sim 45^\circ$. During the intense events to be studied, the function $j(\alpha)$ is known to approach isotropy about the upward hemisphere [O'Brien, 1962b]. It is during these times of isotropy that the determination of $J(> 10$ keV$)$ may be coupled with $J(> 40$ keV$)$ to establish the energy spectra. Isotropy is required to (a) normalize the particle flux measured by 213A and 213C unambiguously, and (b) provide the verification that $J(> 40$ keV$)$ based on 213A, 213C, and SpL are compatible. The significance of the latter consideration has been treated fully in Chapter III.

V. OBSERVATIONS

During the period from January to March, 1963, several periods of intense particle radiation were observed by Injun III. Four such intense periods, including one or more passes, will be discussed in some detail with regard to the absolute character of the particle radiation present. These passes, identified by the satellite revolution numbers, are listed in Table II. This table lists much of the information regarding date, universal time, the range of local time, L space and altitude traversed by the satellite during the period of interest, and the maximum observed energy flux $F_{max}(E_e > E)$ due to electrons of energy greater than E. This material is presented in Table II for the sake of brevity, and hence will not be repeated in the discussion to follow. Also listed in Table II is the value of L_N, the northern, or high latitude, termination of the trapping region as defined by O'Brien [1963b]. It will be seen that this parameter is a distinct feature evident in most of the passes to be discussed.

This series of passes evidences several relatively new and very interesting features which do not properly lie within the scope of the present investigation. It is difficult, however, to avoid brief mention of these phenomena. We will thus define these phenomena for the purpose of recognition and merely acknowledge their existence when appropriate. A detailed investigation of certain of these phenomena is presently underway and studies of others will soon commence.

One such feature to be observed is the "splash," introduced by O'Brien [private communication]. This is characterized by an extremely shortlived intense increment of particle flux (probably low energy electrons) which appears equally at all local pitch angles. The feature is readily apparent at small pitch angles since the increment of flux is large compared to the flux otherwise detected at $\alpha \approx 50^{\circ}$, whereas the splash is not at all apparent in the trapped flux (i.e., those particles with local pitch angles $\alpha \approx 90^{\circ}$).

A second feature to be noted is what will be termed the "plateau," a region in space in which the particle radiation during these events is most intense and nearly isotropic. The counting rates of the thin-windowed 213's (213A, C, and D) are all relatively uniform within the plateau region. The region is seen to terminate very rapidly at the high latitude edge, usually coincident with L_N.

A third feature, a definite pulsating character of the particle intensity in the range of $0 \lesssim \alpha \lesssim 50^{\circ}$, was observed only during revolution 474. A brief discussion, which should be considered parenthetical only, is included in the discussion of this revolution. It is intended only to emphasize the existence and possible significance of this phenomenon.

A. Revolution 400.

Injun III sliced through L values of 4 through ~ 8 at ~ 1046 UT on 14 January 1963, during which time the satellite was in the sunrise penumbra of the earth. The magnetometer indicated satellite alignment to be within three degrees with the local $\underline{B}$ vector throughout the event. The altitude and range of $\underline{B}$ traversed were such that all precipitated particles observed during this pass must have had local pitch angles less than $\sim 57^{\circ}$. Hence, the detector group at $\Theta = 130^{\circ}$ is certainly responding primarily to precipitated particles. We will therefore refer to the responses of the 90° detectors as being due to only trapped particles, and the response of the 130° and 180° detectors as being due to precipitated particles. The counting rates of these detectors are shown in Figure 8 as a function of the on-board clock.

The flux detected is probably due to electrons, since the proton detector PNC-1 at $\Theta = 90^{\circ}$ indicated less than $\sim 5 \times 10^{2}$ protons of $E_p \gtrsim 1$ MeV and the higher energy channels registered no counts during the peak flux. The PN detectors at $\Theta = 180^{\circ}$ also registered no counts during this time. Light contamination of the DC scintillator amounted to about three times the dark current. The peak flux, however, was sufficient to raise the response of DC an order of magnitude above this background level, so that the differential character of the response is not severely obscured during the peak. Photometric observations are not useful during this pass due to atmospherically scattered sunlight [Taylor, private communication].

Revolution 400 represents the most intense event surveyed by Injun III during the six months since launch, but may only be termed moderately intense. The peak energy flux is estimated to be $\sim$20 ergs/cm^2 sec sterad due to electrons of $E_e \gtrsim 10$ keV.

The integral electron spectrum during the event is seen to become progressively softer as the satellite moves northward. This softening is due to both a depletion of the high energy particles ($E_e \gtrsim 250$ keV) as well as an enhancement of the low energy flux. This is depicted in Figure 9 which illustrates the morphology of the integral electron energy spectra during the pass. The first three panels indicate that those electrons present of $E_e \gtrsim 40$ keV detected by the 213's are, in themselves, very nearly sufficient to explain the entire response of the electron multiplier. Thus the particle flux of electrons of energy $10 \leq E_e \leq 40$ keV during the early portion of this event is seen to be less than about one-half that due to electrons of energy $40 \leq E_e \leq 250$ keV. During later portions, the contribution of low energy electrons to the flux is quite evident while, concurrently, the flux of high energy particles

$J(>250$ keV) appears to progressively diminish.

The large increase in the response of both EM and DC between frames 1800 and 1850, during which time SpL (which is not driven beyond its linear region) increases only slightly, indicates an extreme enhancement of the very low energy component just prior to the termination of the plateau region. The progressive decrease of the ratio DC/EM during this period is further testimony to the increasing softness of the spectrum. Typical values of E_o derived from SpL/SpH during the event are shown in Figure 10. The corresponding values of γ derived for the power law spectral model are generally between 2 and 4.

The spectrum during the splashy period prior to the plateau is generally slightly softer than after the plateau, but on the basis of revolution 400 alone there is certainly no great statistical significance to this trend. The spectral character of adjacent peaks and valleys of the splashes shows no such apparent trend toward change of SpL/SpH either before or after the plateau.

The high latitude termination for this pass forms the northern boundary of the plateau region. This is located at $L_N \sim 5.75$, and is seen in the vicinity of frame 1860 of Figure 8. The response of the thin-windowed geiger tubes drop rapidly in a period of about five seconds. The relative decrease is most pronounced in the 90^o and 130^o detectors as compared with the 180^o detector, but all decreases amount to a factor of $\sim$100 - 1000 in this interval. This feature is evident for all particles of energy 10 keV $\leq E_e \leq$ 100 keV, since 213A, C and D, as well as SpH and EM respond in a somewhat similar manner. The sharp termination is not at all evident for particles of $E_e \gtrsim 250$ keV, however, for the 213B shows a gradual decline commencing around frame 1800 and continuing through frame 1880, evidencing an overall decrease by a factor of 50 during this time.

It is of interest to compare the relative magnitude of the variations in flux at pitch angles of $\alpha = 0^\circ$, 50°, and 90° occurring at the termination with those variations occurring during the splashes. At the termination of the plateau, the greatest change of response was apparent in the 213A at 90°, whereas the relative changes during splashes are most apparent in the 213C and D at $\alpha = 50^\circ$ and 0° respectively. The variability of trapped radiation thus appears to be greater at the plateau termination than during the splashes, whereas the opposite is true of precipitated particles.

It should be noted in passing that, associated with this intense flux of electrons, there was significant VLF activity. This activity was characterized by intense chorus prior to the termination, which was replaced by wide-band hiss immediately following the termination [Gurnett, private communication]. As noted earlier, no auroral observations were possible during this pass.

B. Revolution 401.

The satellite passed through nearly the same region in B, L space during both revolution 400 and 401, hence it is possible to observe the changes evident in this region over the 2-hour interval between passes. Local time at the satellite was 0503-0619, hence the DC scintillator and all photometers were sufficiently contaminated by sunlight to obscure all data of interest. The 130° detectors again responded primarily to precipitated particles.

The count rates of the 213 geiger counters are shown in Figure 11. It is evident that the intensity observed during the previous pass has decreased markedly. The peak energy outflux is no greater than ~ 0.2 erg/cm^2 sec sterad.

The spectral observations that are possible during this event indicate the same general dependence on L evident during the previous pass. Compared with revolution 400, the present spectra appear slightly harder at low L values, but considerably softer at the higher L values. Due to the relatively low intensity observed, the counting rate of EM is ~ 0.1/sec. The spectra derived from SpL/SpH therefore utilize averages of SpL/SpH over approximately 10-second intervals of time. It may, however, be stated with certainty that the spectrum in the energy range $40 \leq E_e \leq 100$ keV shows greater softening as the satellite moves to higher L values. The values of E_o and γ observed during this pass vary between $E_o \sim 60$ keV ($\gamma \sim 1$)

at lower L values to $E_o \sim 10$ keV ($\gamma \sim 7$) at the higher L values.

The distinctive morphological feature of the spectra evident in revolution 400, i.e., the great enhancement of the low energy electron flux near the termination is not evident during revolution 401. The 213B response is certainly comparable with the observations of revolution 400. The spatial structure (if the structure is indeed spatial) appears much less pronounced than during the previous pass, and the lack of low energy particles and the high latitude termination cause the zone to appear to have "melted" into a more diffuse and less intense structure during the interim period between revolutions. Figure 11 indicates that such clear-cut features as the termination and the plateau region evident during revolution 400 have been eroded away. The increase of flux evident in all counters does, however, indicate the location of the remnant storm time features.

It is probably reasonable to conclude that, in a general way, the zone has expanded toward higher L values and that the splashy, turbulent nature of the upper portion of the zone has also moved outward, extending now to L values as high as ~ 15. These statements are certainly more true of the low energy ($E_e \gtrsim 40$ keV) electron flux than of the higher energy flux. The higher energy particle structure, based on $J(E_e \gtrsim 250$ keV) determined by 213B, appears to retain the character of revolution 400 quite well, reaching a broad maximum of $J(E_e \gtrsim 250$ keV$) \sim (2\text{-}3) \times 10^4/\text{cm}^2$ sec sterad at $L \sim 5$. No VLF or auroral emissions were observed during revolution 401.

C. Revolution 474.

Revolution 474 is included in this report of the observations primarily because it is a good example of what shall be termed for immediate purposes the phenomenon of pulsating splashes or simply pulsations. Several spectral observations utilizing EM are also possible. The satellite again sliced through a range of L values of 5.5 through 10.0 in a period of about 2 minutes at $\sim$0958 UT on 20 January 1963. Other parameters of interest are listed in Table II. Alignment is considered to be good within $\sim 3^\circ$, and the values of $\underline{B}$ traversed were such that the broadest dumping cone extended to $\alpha \sim 64^\circ$.

Although the sun was not shining on the satellite during this time, the light of sunrise was sufficient to raise the background level of the DC scintillator and the photometers a factor of three above dark current. The event is not energetic enough to activate these detectors significantly above this relatively low contamination level.

The peak flux observed during this event occurs at $L \sim 6.3$ and is estimated to be ~ 0.2 erg/cm^2 sec sterad on the basis of an average electron energy of 40 keV and an integral flux $j(E_e > 10$ keV$)$

$\sim$(2-8) x 10^6/cm^2 sec sterad as determined by EM. The proton detectors report no flux greater than $\sim 10^2$/cm^2 sec sterad due to protons of energy $E_p \gtrsim 1.2$ MeV.

Since this event, as revolution 401, is not of great intensity and the response of EM is low, $\sim$ 0.1 cps, the spectral measurements of the very low energy electrons with EM must thus be considered averages over the period of one or more pulsations. However, if, for example, one were to accept the peak count rate of 213C during a one-second interval commencing at frame 4725 as the average flux observed over the interval from 4718 to 4758, the resulting determination of J($>$40 keV) may certainly be considered an upper limit since it is based on the maximum 213C count rate observed during the entire interval over which EM is averaged. During this interval, EM registered an average flux of $j(E_e > 10$ keV)$\sim$ 2 to 8 x 10^6/cm^2 sec sterad, and 213C indicated $j(E_e > 40$ keV) $\sim$4 x 10^5/cm^2 sec sterad. The slope of this spectrum is quite likely to be somewhat steeper, however, since the flux measurement at 10 keV is considered to be a lower limit of the 10-second averaged flux whereas the flux estimate at 40 keV is considered to be an upper limit.

A few additional samples of electron spectra with points at 10 keV may be constructed in the same manner as the above. These indicate that the integral spectra between 10 and 40 keV become quite flat during the event in contrast to the pattern noted in revolution 400. The sample available at $L \sim 9$ indicates $J(>10 \text{ keV})$ is at most a factor of 2 to 3 greater than $J(>40 \text{ keV})$, while this same ratio for the earlier example was about a factor of 10. The ratio SpL/SpH throughout the pass shows a slight tendency to decrease at higher L values, also indicating a hardening of the spectrum.

The pulsating character evident in this pass is clearly visible in Figure 12. It should be pointed out that the pulsations are to be contrasted with the splashes mentioned earlier on the basis of (a) the "pulse width" of the flux enhancement, and (b) the repetitive nature of the enhancements. Comparison of the splashes apparent in revolution 400, Figure 8, with those of revolution 474 illustrates that the two phenomena are indeed different in both respects. On the basis of the peak-to-peak spacing in time, the 12 distinct pulsations display average period of 7.9 seconds. The standard deviation of the data is 2.2 seconds, hence the distribution of periods is 7.9 ± 2.2 seconds at a confidence level of ~ 0.7 during this interval of time.

A comparison of the ratio SpL/SpH for all peaks and all valleys indicate no significant spectral distinction between the pulsating and non-pulsating components in the energy range $40 \lesssim E_e \lesssim 100$ keV. 213B is counting far too low to yield adequate statistics, and hence we may only state that the spectral character of the pulsations, although quite evident in the low energy component, may or may not be evident in the higher energy components. It is interesting to note that the classical zone-like structure of high energy electrons as detected by 213B lies almost completely to lower L values than the transient phenomenon discussed above.

Schematically, this pass evidences the same general structure as that apparent in the previous event discussed. The plateau region is sharply bounded on the northern side at $L \sim 8$, extending to this value from $L \sim 7$. Both to the south and to the north of the plateau region one may observe the time variable structure which was previously evident as splashes rather than pulsations as in the present case. The progressively decreasing count rates evident by visualizing the envelope of the peaks and the plateau merits speculation. Although this may well be due either to the mirror point distribution on the various L shells as the satellite moves toward higher $\underline{B}$, or a pure L dependence, another possible cause may be that loss mechanisms are progressively degrading the total particle content of the zone. It is therefore conceivable that these features may be either temporal or spatial. Speculation regarding the spatial or temporal origin of these pulsations would certainly be of great interest, but will not be dealt with at this time.

Auroral data are not of significance during this revolution because of sunlight contamination of the photometers.

The VLF detector indicated no activity of interest above the noise level of the apparatus.

D. Revolution 609.

Revolutions 609 and 610 provide a second opportunity to survey twice in a two-hour interval the features of an intense event in the outer zone at essentially the same location in B, L space. During revolution 609, the satellite passed through L values of 4 to 7 in an interval of 2 minutes around 0707 UT on 31 January 1963. Both the DC scintillator and the photometer are potentially useful during the event during the early portion of the pass, but the satellite entered sunlight at 0210 local time, near the end of the pass. The magnetometers indicated alignment of the satellite with respect to local $\underline{B}$ was within $\sim 5^{\circ}$. The location in $\underline{B}$ space was such that the broadest dumping cone extended out to $\alpha \sim 67^{\circ}$. The 130° detector group is thus indicating precipitated particles. The field of view of the 90° detectors may overlap the extremity of the dumping cone by as much as three or four degrees as the satellite oscillates. This effect need not concern us, however, since the isotropy observed during these events will make such an overlap inconsequential to our present purposes.

The counting rates of the detectors are shown in Figure 13.

As in the previous pass, the flux detected is probably due to electrons since the PN junction detectors indicate the proton flux $J(E_p \gtrsim 1 \text{ MeV}) \lesssim 3 \times 10^3/\text{cm}^2$ sec sterad with pitch angles of 90°. No protons are apparent at $\theta = 180^\circ$. The peak flux, observed at $L = 5.5$, is estimated to be $\sim 1 \text{ erg/cm}^2$ sec sterad due to electrons of $E_e \gtrsim 10$ keV, assuming an average electron energy of 20 keV.

The integral energy spectrum of the precipitated particles may be observed with excellent statistics in the plateau region of this event. Selected spectra are shown in Figure 14. The trend toward softer spectra as the satellite moves to higher L values is again quite evident. This series of panels also indicates the limits of applicability of the exponential spectral model. The first two spectra strongly indicate a power law form to be more accurate, since the slope appears to increase in absolute value toward lower energies in contrast to the decrease of slope expressed in the exponential form. The increasing slope at lower energies gives the spectra the appearance of "blowing up" at still lower energies. During the latter portion of the pass, however, the exponential model becomes more applicable and the curves show a degree of flattening at low energy, which may be interpreted to indicate that a turn-over point in the differential spectra does exist. The softening of the spectra is not observed to be due to the increase of low energy particles as was observed in revolution

400 since $J(E_e \gtrsim 10 \text{ keV})$ does not increase markedly during the pass. Instead, the higher energy component indicated by 213B decreases, as does the integral point derived from SpH in the manner described in a previous section.

The ratio of SpL/SpH also reveals a marked softening of the spectrum, with typical values of E_0 decreasing from 25 keV to a minimum of 7 keV. Corresponding values of γ range from 2 to 7. The variability of these spectral parameters is, as before, large and rapid.

The high latitude termination of the plateau occurs at $L_N \sim 5.5$. The most extreme decrease is shown by 213D at $\theta = 180^\circ$. This is somewhat less than that evident during revolution 400, but still amounts to a factor of 100. The 90° and 130° geigers respond similarly, but decrease by only a factor of $\sim$10 in a period of 5 seconds ($\Delta L \lesssim 0.1$). These decreases are evident in SpH, the thin-windowed geigers, and EM, whereas 213B decayed slowly in the southern portion of the plateau region. The termination thus appears to be a low energy phenomenon. The total decrease of 213B was a factor of 50 or more during $\sim$30 seconds, corresponding to a ΔL of $\sim .75$.

Associated observations during revolution 609 of auroral and VLF phenomena indicate the presence of both. The photometer, however, was just coming into sunlight as the auroral buildup was occurring. It is thus difficult to estimate the intensity [Taylor, private communication]. VLF activity was characterized by auroral hiss, but has not yet been analyzed in detail. Such an analysis is anticipated [Gurnett, private communication].

E. Revolution 610.

Revolution 610 traversed L values of 4 through 11 during a three-minute interval commencing at 0903 UT, 31 January 1963. Alignment of the satellite was within 4° throughout and the local dumping cone extended out to $\alpha \sim 69^{\circ}$. Contamination of the 90° detectors by fluxes other than trapped is possible but, as for the previous pass, the general isotropy of these fluxes renders a distinction between trapped and precipitated fluxes unnecessary. The 130° detectors are, however, certain to observe precipitated fluxes only.

A great deal of potentially interesting information during revolution 610 is missing due to noise at the receiving station, as is evident in Figure 15. An estimate of the maximum precipitated flux is ~ 2 ergs/cm^2 sec sterad on the basis of the count rates in the vicinity of frames 5050 - 5075. The features of interest discussed for the previous passes are lacking in significance in the present instance, so an extremely brief qualitative discussion will instead be presented.

The spectral character of revolution 610 also indicates generally softening spectra in the range of L between L = 6.5 and L = 11; values of E_o derived from SpL/SpH are somewhat harder than previously observed, varying between 35 keV and 12 keV. The corresponding values of γ range from 2 to 4.5. The splashy features are qualitatively very similar to those discussed previously in the region of $L > L_N$. No plateau is evident, but this may well be due to the lack of data. The plateau, if it exists, is probably located in the region $L \sim 7$.

The changes evident in revolution 610 since the previous pass indicate that although the peak intensity has not noticeably decreased, the entire zonal structure has apparently expanded toward both higher and lower L values. If any conclusions regarding the termination are warranted, it must be said that the sharp features have been eroded, the entire structure becoming somewhat more diffuse and extended in space. This effect is similar to that observed in revolution 401.

Both auroral [Taylor, private communication] and VLF [Gurnett, private communication] emissions were present during revolution 610, but reception difficulties during the early, and most intense, portion of the pass were sufficient to obscure much of the data.

F. Revolution 994.

Revolution 994 is of interest because it affords the opportunity of examining the energy spectrum and angular distribution during a single, shortlived burst of precipitated particles which coincide in space and time with a visual aurora. The entire event occupies less than one minute at 0721 UT on 3 March 1963. Local time of the satellite was $\sim$2220 and the L value of this event was 8 to 10. The satellite was aligned with $\underline{B}$ within $\sim 3^{\circ}$, and the magnitude of $|\underline{B}|$ was such that the edge of the dumping cone extended out to $\alpha \sim 80^{\circ}$. Hence the 130° and 180° detector groups respond only to precipitated particles. The satellite was in the earth's shadow, and thus no contamination of the DC scintillator or photometers was evident. No protons of $E_p \gtrsim 1$ MeV were detected by the PN junction detectors at either $\theta = 90^{\circ}$ or $\theta = 180^{\circ}$.

Figure 16 shows the counting rates of the 213A, C, and D, EM, and the 3914Å photometer oriented at 0° so as to respond to auroral light generated in the atmosphere at the base of the field line. The correlation of these phenomena is seen to be quite good.

The precipitated energy flux due to electrons of $E_e \gtrsim 10$ keV is estimated to be $\sim$2 ergs/cm^2 sec sterad. The electron energy spectrum of the event is much steeper than any observed previously with Injun III. As can be seen from Figure 17, the ratio $J(>10 \text{ keV}) / J(>40 \text{ keV})$ was observed to be greater than 500.

Such a slope corresponds to a value of $E_0 = \sim 4$ keV, or a γ of ~ 7. The integral spectra require that the power law spectral model be used to designate the shape of this spectra throughout the event. Assignment of a value of γ may be done with good accuracy on the basis of SpL/SpH since the power law-model appears to hold well to electron energies of 100 keV.

The first two panels of Figure 17 do not indicate any change of spectra evident during this short period, but it may be seen from Figure 16 that EM indicated a decrease of flux prior to that indicated by 213C. This indication is taken to be real since the DC scintillator also showed a decrease at the same time. The ratio SpL/SpH also indicates no trend toward softening spectrum. It is thus concluded that any progressive spectral change present is due to flux variations of 10 - 40 keV electrons.

The angular distribution of this event is seen to be quite isotropic throughout the one-minute interval. The directional fluxes detected by 213A, C, and D indicate complete isotropy of flux (within 50%) at pitch angles $\alpha = 0^{\circ}$ through $\alpha = 90^{\circ}$. This may be noted by comparing the fluxes reported by these detectors as indicated in the integral spectra of Figure 17.

The temporal or spatial structure observed during this pass indicates the time scale of the event to be ~ 25 seconds or the spatial extent of the structure to be ~ 100 km. It is not purposeful at this point to consider which structural parameter is the more significant. The high latitude termination of the plateau, if we can consider a plateau to exist, is located at $L_N = 10$. The width of this plateau is $\Delta L \sim 1.5$, and thus is similar in this respect to the plateaus noted during previous passes.

Both auroral and VLF activity were detected simultaneously. The auroral emission associated with this event is described by Taylor [private communication] as intense, amounting to ~ 20 kilo-rayleigh of 3914Å emission. VLF activity is characterized by the presence of auroral hiss. The relation between particle, auroral, and VLF phenomena is to be reported in detail by Gurnett [1963].

VI. DISCUSSION AND CONCLUSION

The four intense events described in the previous section afford the opportunity to observe the energy spectra and fluxes of 10 keV electrons within the outer zone during periods of disturbance. It will be the purpose of this discussion to point out the general character of the L profiles obtained during these passes and the behavior of the low energy electron flux within the outer zone, and to comment on these measurements with regard to the results of previous investigations.

An examination of Figures 8, 11, 12, 13, 15, and 16, which present the counting rates of selected detectors as a function of time (and location in L), reveals a pattern in which all passes display certain features in common. It will be of interest to reiterate this generalized structure briefly.

The structural pattern is characterized by a plateau region of relatively constant counting rate which is bounded on both north and south by regions in which sharp spikes of large magnitude occur. This pattern is most noticeable in the 130° and 180° detectors. Revolution 474 displays this pattern with the modification that the plateau, instead of being of constant counting rate, is characterized by a region of monotonically decreasing counting rate. The uniformity of the count rate evident on these plateaus belies, to some extent, the magnitude of the transients in flux because the geigers are operating in the non-linear region of response, hence large changes of flux may be represented by only small changes in the apparent counting rate. That such a plateau does exist as a region in which the flux is relatively constant is claimed on the basis of the following reason. The plateau feature has been observed (revolution 474) at relatively low counting rates of $\sim$250 counts/frame in the 213D, and less than 150 counts/frame in the 213C. These rates are well below the peak rates of 420 and 600 counts/frame, respectively. Thus, although the tubes are driven into the non-linear region, they are far from saturation and hence are not distorting the magnitude of the flux variations by more than 20% in this instance.

The phenomenon discussed by O'Brien [1963b] of the high latitude termination of trapping in the outer zone is obvious in several of these passes. Although detailed consideration of this termination is not necessary to this investigation, the existence of this feature will be of use later. The termination, for the immediate purpose, is taken to be the northern boundary of the plateau region, but this definition, during the intense events observed, does not alter the value of L_N as determined by O'Brien. The termination is characterized by a distinct, sudden decrease of the counting rates of all detectors with energy thresholds less than $\sim$100 keV, but not evident in the 213B, whose threshold is 250 keV for electrons. The L value of this termination is seen to be 5.7, $\sim$8, and 5.5 in revolution 400, 474, and 609 when the location may be determined accurately. These values are at somewhat lower L values than those reported by O'Brien, but agree well with the observation that L_N appears at lower L values during intense events. Revolutions 610 and 994 display values in very good agreement with those of O'Brien. It should be noted that this termination occurs simultaneously for particles of all pitch angles $0^{\circ} \leq \alpha \leq 90^{\circ}$, as well as for particles of energy $10 \leq E_e \leq 250$ keV. The distinct high latitude termination is not evident in the fluxes of electrons of $E_e \gtrsim 250$ keV as reported by 213B.

The integral electron energy spectra during these events have been observed within the plateau to be widely variable within any single event as well as from one event to another. This feature has, of course, been reported previously by a large number of investigators. Interpretations of some previous experiments within the outer zone have shown that the spectrum generally continues to increase, apparently without limit, toward lower and lower energies. It is proposed that the interpretation of the several detailed spectral samples obtained with Injun III within the outer zone indicate that, in some (but not all) cases, the differential number-energy distribution does not continue to increase throughout the range of energies between 10 and 40 keV. This contention rests upon the integral flux measurements obtained with the electron multiplier and the thin-windowed geiger tubes.

Consider the spectra displayed in Figure 9 which were obtained during revolution 400. As noted earlier the spectral variations that occurred during the plateau region as the satellite moved northward were due to (a) the steady decline of particle flux due to electrons of energies $E_e \gtrsim 250$ keV prior to the termination, as well as (b) the rapid increase just south of the termination of the low energy electron flux. The relative depletion of the low energy component early in the plateau is shown in the first few panels of Figure 9. It is seen that an apparent low energy end point of these spectra must lie somewhere between 10 and 40 keV, since it is evident that the total flux detected by the electron multiplier is only very slightly greater than that indicated by the thin-windowed 213's. The steady increase of $j(>10$ keV$)$ determined by EM (and also, in a qualitative manner, by DC) indicates that the flux between 10 and 40 keV is enhanced as the satellite nears the termination point.

Spectral observations of the flux within the plateau region observed during revolution 609 indicate a somewhat different morphology. Initially, the spectrum is relatively hard and definitely resembles a power law function. As the satellite proceeds northward, the 10 and 40 keV integral points increase while the 100 and 250 keV points decrease, yielding the net effect of a softening spectrum. The final spectral shape is definitely similar to the exponential form for energies $\gtrsim 250$ keV. The initial form shows no clear indication of a turnover point, but the final panel does so indicate. It appears likely that the differential distribution has passed through a maximum and is declining toward lower energies, but it cannot be stated whether or not the maximum occurs above or below 40 keV.

It would be of interest to investigate in additional events the spectral variation within the plateau as the satellite approaches the termination. Revolution 474 is the only other pass included in the present discussion that evidences a sharp termination, but because of the diminished intensity of this pass, only a few spectral determinations may be made. The indication is that the general pattern of the spectra between 10 and 40 keV tends to flatten slightly as the satellite moves northward. The spectra of revolution 474 also show indication that a turnover point is likely to exist, but again it is not conclusively between 10 and 40 keV.

An alternative method of summarizing these data is shown in Figure 18, where the ratio of directional electron fluxes $j(>40 \text{ keV})/j(>100 \text{ keV})$ is plotted against the ratio $j(>10 \text{ keV}) / j(>40 \text{ keV})$. These two ratios were observed during the plateau regions of the revolutions indicated, and are taken as a measure of the relative steepness of the spectrum between the limits specified.

The location of each point indicates the uniformity of slope of the integral spectrum in each of the two regions $10 \leq E_e \leq 40$ keV and $40 \leq E_e \leq 100$ keV respectively. The straight lines indicate the ratios to be expected if the observed spectra obeyed either a power law or an exponential model. Numerical values of the shape parameters γ and E_o respectively are indicated on these lines. The points located below the power-law line are those which may be identified with spectra which definitely display an increasing differential number-energy distribution function. Those points which appear above this line as well as those appearing near the exponential line represent spectra in which the slope between $40 \leq E \leq 100$ keV is greater than the slope between $10 \leq E \leq 40$ keV, i.e., those spectra whose differential functions do not display the rapid increase at lower energies which is characteristic of the power-law forms. It will be noted that the scatter of points is large, but that they are approximately equally distributed between the power-law and exponential forms.

It is thus claimed that several measurements of electron spectra do indicate that the differential energy distribution function characterizing the electron flux at high latitudes during intense events does not continue to increase toward lower energies in the range $10 \leq E_e \leq 40$ keV. An apparent maximum in the differential function has been observed to lie near 40 keV on at least one occasion. It is also considered likely that the maximum may well lie between 10 and 40 keV in several of the spectra examined. These results are in reasonable accord with the report of Cladis et al. [1961], for instance, which demonstrates also that the differential function does not continuously increase toward lower energies in the range $50 \leq E_e \lesssim 600$ keV.

There are instances, however, that indicate conclusively that this maximum must lie below 10 keV. Consider the spectral representations of Figure 17 for revolution 994. This event displays the steepest electron energy spectra yet observed by Injun III, and is associated with intense auroral and VLF activity. The spectra presented rise very sharply between 40 and 10 keV, requiring that if a maximum in the differential spectrum exists, it exists below 10 keV. This observation indicates that, on this occasion, the mean energy of electrons responsible for visible aurora is below 10 keV. McIlwain [1960] has estimated the mean energy to be $\sim(10 \pm 5)$ keV. It is of interest to recall the measurement reported by Davis et al. [1960] which indicated, during an auroral event, $j(30 \text{ eV} \leq E_e \leq 1 \text{ keV}) \lesssim 10^9/\text{cm}^2$ sec sterad, but $J(E_e > 8 \text{ keV}) \sim 2 - 6 \times 10^7/\text{cm}^2$ sec sterad.

This report might also be taken as an instance in which differential spectrum did not increase rapidly toward lower energies in the range 1 keV$\leq E_e \leq 8$ keV.

The preliminary estimate of the intensity of 3914Å auroral light emitted during revolution 994 is $\sim$20 kilorayleighs [Taylor, private communication]. Assuming the observed directional electron flux at the satellite is isotropically incident on the atmosphere below, the efficiency for production of auroral light by electrons of $E_e \gtrsim 10$ keV is $\sim 0.7\%$, in fair agreement with McIlwain's [1960] efficiency estimate of $\sim 0.2\%$.

The electron fluxes and spectra reported here are generally in good agreement with the observations of others. Previously cited reports of very low energy electron fluxes lie in the range $10^7 \leq j(E_e \gtrsim 10 \text{ keV}) \lesssim 10^{10}/\text{cm}^2$ sec sterad with a variety of values of E_o between 4 and 22 keV. The observations reported here are in the range $2 \times 10^6 \leq j(>10 \text{ keV}) \lesssim 10^9$. The values of E_o based on SpL/SpH were found to be ~ 4 to ~ 25 keV. Values of E_o or γ based on $J(>10 \text{ keV}) / J(>40 \text{ keV})$ vary widely because of (a) the instances in which this ratio is ~ 1, observed during revolution 400, and (b) the extremely steep spectra observed during revolution 994, when E_o, if applicable, would have been 3 keV, and γ was ~ 4.

The temporal variations of the electron energy spectrum during an intense event in the outer zone have previously been reported to be disordered and widely variable. These results are also evident here. It may be of interest, however, to examine the spectral characteristics for a possible spatial dependence. One method by which this may be done is shown in Figure 19, which presents a plot of the ratio of directional fluxes, as defined above, as a function of the quantity $L_N - L$. This latter quantity might be thought of as representing the position of the satellite (in units of L) south of the high latitude termination, and thus within the plateau region. It is obvious from Figure 19 that the spectral behavior within the plateau region is equally as disordered in spatial structure as it is in temporal structure.

The essential findings of the present investigation with regard to the energy spectrum of electrons of energies 10 keV $\leq E_e \lesssim 1$ MeV are as follows. First, it is found that neither the power law nor the exponential form of spectral model fits these data well. Second, the accuracy of either model is widely variable within a single pass, and that these variations are probably neither purely spatial nor temporal in origin. Third, these observations indicate that the differential number-energy distribution function of electrons does not always continue to rise toward lower energies in the range $10 \leq E_e \leq 40$ keV. In addition to these features regarding the electron energy spectrum, the outer zone during these intense events was found to evidence several structural features in common. The first of these is the splash phenomena or pulsations evident in the flux of electrons of $E_e \geq 40$ keV. The second of these is the plateau feature with its sharply defined northern termination point.

The six revolutions of Injun III reported herein all present the opportunity to measure the flux of low energy electrons within the outer zone. These six occasions approach in number the total number of previously reported observations of electrons of energy between 10 and 40 keV within the outer zone. These observations are also the first such observations (to the knowledge of this author) to be reported based on the use of an electron multiplier as a low energy electron detector. Further, the electron multiplier aboard Injun III has demonstrated that such a detector is indeed feasible for satellite use. Despite the sensitivity of a multiplier structure to the effects of atmospheric contamination and the other sources of gain degradation, no such deterioration of the multiplier performance occurred prior to launch. The multiplier gain has also been demonstrated to be stable within 10% during the lifetime (to date) of the satellite.

A possible future application of an electron multiplier would be in the investigation of the very low energy (100 eV $\lesssim E_e \lesssim$ 50 keV) electron fluxes within the outer zone. Such a detector, utilizing a high gain pulse amplifier for the detection of individual particles, would enable one to map the intensity contours of these low energy particles in space. Another possible application would be in an experimental investigation of the process by which the outer zone is populated. It is known, for example, that the loss rate of electrons from the outer zone during times of intense precipitated fluxes is sufficient to completely empty the outer zone within a few hours [O'Brien, 1962a]. The source of outer zone electrons must therefore be quite strong. Several source or acceleration mechanisms as discussed by Kaufman [1963] imply that very low energy electrons are of considerable importance in these processes. A third possible application would be in the investigation of the nature of the solar plasma clouds known to occupy interplanetary space. These problems, as well as many others, require knowledge of the very low energy particles that can be provided by an electron multiplier.

Table I

Injun III Detector Complement

Detector	Symbol	Orientation*	Detectable Radiation	
			Proton Energies	Electron Energies
213 Geiger Counter	213A	$\theta = 90^{\circ}$	$E \gtrsim 0.5$ MeV	$E \gtrsim 40$ keV
Pulse Scintillator		Omnidirectional	$E \gtrsim 40$ MeV	--
213 Geiger Counter	213B	$\theta = 90^{\circ}$	$E \gtrsim 4$ MeV	$E \gtrsim 250$ keV
213 Geiger Counter	213C	$\theta = 130^{\circ}$	$E \gtrsim 0.5$ MeV	$E \gtrsim 40$ keV
213 Geiger Counter	213D	$\theta = 180^{\circ}$	$E \gtrsim 0.5$ MeV	$E \gtrsim 40$ keV
302 Geiger Counter	302	Omnidirectional	$E \gtrsim 20$ MeV	$E \gtrsim 1.5$ MeV
Magnetic (a)	SpL		--	$42 \leq E \leq 53$ keV
Electron (b)	SpH	$\theta = 90^{\circ}$	--	$83 \leq E \leq 98$ keV
Spectrometer (c)	SpB		$E > 40$ MeV	$E \gtrsim 12$ MeV
D.C. Scintillator	DC	$\theta \sim 130^{\circ}$	$E \gtrsim 50$ keV	$E \gtrsim 5$ keV
Electron Multiplier	EM	$\theta \sim 130^{\circ}$	$E \gtrsim 50$ keV	$E \gtrsim 5$ keV

Table I (continued)

Detector	Symbol	Orientation*	Detectable Radiation	
			Proton Energies	Electron Energies
P-N Junction (a)	PNA	$\Theta = 90^{\circ}$	$1 < E < 2$ MeV	--
P-N Junction (b)	PNB	$\Theta = 90^{\circ}$	$2 < E < 8$ MeV	--
P-N Junction (c)	PNC	$\Theta = 180^{\circ}$	$8 < E < 26$ MeV	--
P-N Junction (d)	PND	$\Theta = 180^{\circ}$	$26 < E < 100$ MeV and two backgrounds for each pair	--
Photometer (a)		$\Theta = 0^{\circ}$	Light of 5577Å	
Photometer (b)		$\Theta = 0^{\circ}$	Light of 3914Å	
Photometer (c)		$\Theta = 180^{\circ}$	Light of 5577Å	
VLF Detector	VLF		VLF 1 kc/s to ~ 9 kc/s in 6 Frequency Bands and Carrier Modulation 1 to 7 kc/s	
Integral (a)	IsL	$\Theta = 90^{\circ}$	$E \gtrsim 4$ MeV	$E \gtrsim 1.3$ MeV
Magnetic (b)	IsH	$\Theta = 90^{\circ}$	$E \gtrsim 4$ MeV	$E \gtrsim 3$ MeV
Spectrometer (c)	IsB		$E \gtrsim 40$ MeV	$E \gtrsim 12$ MeV

Table I (continued)

Detector	Symbol	Orientation*	Detectable Radiation
			Sunlight incident within a cone of angular diameter
Solar Aspect Sensors	S^1	$\theta = 90^\circ$	70°
	S^2	$\theta = 130^\circ$	70°
	S^3	$\theta = 180^\circ$	120°
	S^4	$\theta = 90^\circ$	70°
	S^5	$\theta = 130^\circ$	70°
	S^6	$\theta = 90^\circ$	40°
	S^7	$\theta = 130^\circ$	40°

* Orientation is referred to the direction of the magnetic field line, such that $\theta = 0^\circ$ corresponds to a detector looking downwards towards the earth in the northern hemisphere.

Table II

Intense Events Observed by Injun III During January and March, 1963

Date 1963	Revolution Number	Universal Time	Local Time	L	Altitude	L_N (approx.)	Maximum Energy Flux F_{max} ($E_e \gtrsim 10$ keV)
14 Jan.	400	1045	0447 -0528	4-8	750 ± 100 km	5.4	~ 20 ergs/cm^2 sec sterad
14 Jan.	401	1245	0503 -0619	4-10	520 ± 70		~ 0.2
20 Jan.	474	0958	0408 -0440	6-10	570 ± 20	~ 8	~ 0.1
31 Jan.	609	0706	0146 -0222	4-7	500 ± 65	5.5	~ 1
31 Jan.	610	0904	0158 -0257	4-11	390 ± 70	(10.5)	(2)
3 Mar.	994	0721	2207 -2236	8-10	285 ± 15	10	~ 2

REFERENCES

Allen, J. S., "An Improved Electron Multiplier Particle Counter", Rev. Sci. Instr. 18, No. 10, 739 (1947).

Bruining, H., Physics and Applications of Secondary Electron Emission, McGraw-Hill Book Co., New York (1954).

Cladis, J. B., L. F. Chase, W. L. Imhof, and D. J. Knecht, "Energy Spectrum and Angular Distributions of Electrons Trapped in the Geomagnetic Field", J. Geophys. Research 66, 2297-2312 (1961).

Curran, S. C., Luminescence and the Scintillation Counter, Butterworth's Scientific Publications, London (1953).

Davis, L. R., O. E. Berg, and L. H. Meredith, "Direct Measurements of Particle Fluxes in and Near Auroras", pp. 721-735, Space Research, Proceedings of the First International Space Science Symposium, edited by H. Kallman Bijl, North Holland Publishing Co., Amsterdam, 1960.

Davis, L. R., and J. M. Williamson, "Low Energy Trapped Protons", GSFC Preprint X-611-62-89 (1962).

Farley, T. A., "The Growth of Our Knowledge of the Earth's Outer Radiation Zone", Reviews of Geophysics 1, 3-34 (1963).

REFERENCES (continued)

Fisher, P. C., A. J. Meyerott, H. A. Grench, R. A. Nobles, and J. B. Reagen, "Soft Particle Detectors", IEEE Transactions on Nuclear Science NS10, 211 (1963).

Forbush, S. E., G. Pizzella, and D. Venkatesan, "The Morphology and Temporal Variations of the Van Allen Radiation Belt, October 1959 to December 1960", J. Geophys. Research 67, 3651-3668 (1962).

Frank, L. A., "Efficiency of a Geiger-Mueller Tube for Non-Penetrating Electrons", J. Franklin Institute 273, 91-106 (1962).

Frank, L. A., J. A. Van Allen, W. A. Whelpley, and J. D. Craven, "Absolute Intensities of Geomagnetically Trapped Particles with Explorer XIV", J. Geophys. Research 68, 1573 (1963).

Freeman, J. W., "A Satellite Borne Cadmium Sulfide Total Corpuscular Energy Detector", SUI Research Report 61-2, February 1961 (unpublished).

Freeman, J. W., "The Morphology of the Electron Distribution in the Outer Radiation Zone and Near the Magnetospheric Boundary as Observed by Explorer XII", SUI Research Report 63-20, June 1963 (unpublished).

Goodrich, G. W., and W. C. Wiley, "Resistance Strip Magnetic Electron Multiplier", Rev. Sci. Instr. 32, No. 7 (1961).

REFERENCES (continued)

Gringauz, K. I., V. G. Kurt, V. I. Moroz, and I. S. Shklovskii, "Ionized Gas and Fast Electrons in the Earth's Neighborhood and Interplanetary Space", Artificial Earth Satellites 6, pp. 130-136, Plenum Press, Inc., New York, 1961.

Gurnett, D. A., "Very Low Frequency Electromagnetic Emissions Observed with the O.N.R./S.U.I. Satellite Injun III", M.S. Thesis, State University of Iowa, August 1963.

Heroux, L., and H. E. Hinteregger, "Resistance Strip Magnetic Photomultiplier for the Extreme Ultraviolet", Rev. Sci. Instr. 31, No. 3 (1960).

Hirashima, M., and S. Miyashiro, "Some Factors Affecting the Decay of Secondary Electron Emission of Silver-Magnesium Alloys", J. Phys. Soc. Japan 12, 770-777 (1957).

Hoffman, R. A., L. R. Davis, and J. M. Williamson, "Protons of 0.1 to 5 MeV and Electrons of 20 KeV at 12 Earth Radii during Sudden Commencement on September 30, 1961", J. Geophys. Research 67, 5001-5005 (1962).

Kaufman, R., "Experimental Tests for the Acceleration of Trapped Particles", J. Geophys. Research 68, 371-386 (1963).

REFERENCES (continued)

Krasovskii, V. I., I. S. Shklovskii, Yu. I. Gal'perin, E. M. Svetlitskii, Yu. M. Kushnir, and G. A. Bordovskii, "Discovery of Approximately 10-KeV Electrons in the Upper Atmosphere", Artificial Earth Satellites 6, pp. 137-155, Plenum Press, Inc., New York, 1961.

Massey, H. S. W., and E. H. S. Burhop, Electronic and Ionic Impact Phenomena, Clarendon Press, London, 1952.

McDiarmid, I. B., D. C. Rose, and E. Budzinski, "Direct Measurements of Charged Particles Associated with Auroral Zone Radio Absorption", pp. 1194-1205, Space Research II, edited by H. Kallman Bijl, North Holland Publishing Co., Amsterdam, 1961

McIlwain, C. E., "Direct Measurements of Particles Producing Visible Auroras", J. Geophys. Research 65, 2727-2747 (1960).

McIlwain, C. E., "Coordinates for Mapping the Distribution of Magnetically Trapped Particles", J. Geophys. Research 66, 3681 (1961).

O'Brien, B. J., "Lifetimes of Outer-Zone Electrons and Their Precipitation into the Atmosphere", J. Geophys. Research 67, 3687-3706 (1962a).

O'Brien, B. J., "Direct Observation of Dumping of Electrons at 1000 Km Altitude and High Latitudes", J. Geophys. Research 67, 1227-1233 (1962b).

REFERENCES (continued)

O'Brien, B. J., "Review of Studies of Trapped Radiation with Satellite-Borne Apparatus", Space Science Reviews 1, 415-484 (1963a).

O'Brien, B. J., "A Large Diurnal Variation of the Geomagnetically Trapped Radiation", J. Geophys. Research 68, 989-995 (1963b).

O'Brien, B. J., and C. D. Laughlin, "An Extremely Intense Electron Flux at 1000 Km Altitude in the Auroral Zone", J. Geophys. Research 67, 2667-2672 (1962).

O'Brien, B. J., C. D. Laughlin, L. A. Frank, and J. A. Van Allen, "Measurements of Intensity and Spectrum of Electrons at 1000 Km Altitude and High Latitudes", J. Geophys. Research 67, 1209-1225 (1962a).

O'Brien, B. J., J. A. Van Allen, C. D. Laughlin, and L. A. Frank, "Absolute Electron Intensities in the Heart of the Earth's Outer Radiation Zone", J. Geophys. Research 67, 397-403 (1962b).

O'Brien, B. J., C. D. Laughlin, and D. A. Gurnett, "High Latitude Geophysical Studies with Injun III, I. Description of the Satellite", (to be submitted to J. Geophys. Research for publication) (1963).

REFERENCES (continued)

Rosser, W., "Changes in the Structure of the Outer Radiation Zone Associated with the Magnetic Storm of September 30, 1961", J. Geophys. Research 68, 3131-3148 (1963).

Rosser, W., B. J. O'Brien, J. A. Van Allen, L. A. Frank, and C. D. Laughlin, "Electrons in the Earth's Outer Radiation Zone", J. Geophys. Research 67, 4533-4542 (1962).

Rothwell, P., and C. E. Mcilwain, "Magnetic Storms and the Van Allen Radiation Belts: Observations from Satellite 1958 Epsilon (Explorer IV)", J. Geophys. Research 65, 799-809 (1960).

Treloar, L. R. G., "A Method of Measuring Secondary-Electron Emission from Filaments", Proc. Phys. Soc. 48, 488-497 (1936).

FIGURE CAPTIONS

Figure 1. Plan view of the Injun III scientific payload.

Figure 2. Assembly drawing of the front portion of the electron multiplier. The first dynode is mounted on a Kovar ring (A) which is sealed to the glass tube. The tube structure is potted in Silastic rubber (Q), and housed in a magnesium housing (B). Shielding (P and N) consists of .005" Netic magnetic shielding and .010" lead foil. "O" rings (D and M) provide an air tight seal to the front end housing (J). The collimator (E) admits particles, which must pass through the 1000Å nickel foil (G). Both the collimator and the foil holder (K) are of leaded-nickel-silver. Outgassing of the structure is provided for by the open channels (L) around the periphery of the foil holder. The trap door lid seals against the "O" ring (H) to provide an airtight seal so that the entire assembly may be contained within an inert atmosphere.

Figure 3. Schematic diagram of the high voltage power supply and the electrometer associated with the electron multiplier.

Figure 4. Anode current of the multiplier and the corresponding electrometer response for particle influx simulated with a variable intensity light source.

Figure 5. The detector response function D_{EM} of the electron multiplier.

Figure 6. Detailed low energy sensitivity of electron multiplier showing effect of (a) 1000Å nickel foil across the aperture and 2500 volt retarding potential on first dynode, (b) effect of foil alone, and (c) effect of 2500 volt retarding potential

FIGURE CAPTIONS (continued)

alone. Curves are in arbitrary units and are not normalized with respect to one another.

Figure 7. The angular sensitivity function $f_E(\theta)$. All points are normalized to unit efficiency at $\theta = 0^\circ$.

Figure 8. Counting rates of selected Injun III detectors during revolution 400 in counts per frame (1 frame = 1/4 second) as a function of the A frame counter.

Figure 9. Sample integral electron energy spectra observed during revolution 400. See Figure 8 for location of each sample in data.

Figure 10. The spectral shape parameter E_o in the differential form $N(E)dE = N_o e^{-E/E_o}\,dE$ as a function of the A frame counter during revolution 400.

Figure 11. Counting rates of selected Injun III detectors during revolution 401.

Figure 12. Counting rates of selected Injun III detectors during revolution 474. Note particularly the pulsating character of the counting rate of 213C and 213D.

Figure 13. Counting rates of selected Injun III detectors during revolution 609.

Figure 14. Sample integral electron energy spectra observed during revolution 609. Note change of shape from power-law form to exponential form at higher L values.

FIGURE CAPTIONS (continued)

Figure 15. Counting rate of selected Injun III detectors during revolution 610. Lack of data due to noise in the early portion of this pass probably obscures plateau. Note few available points show high counting rates.

Figure 16. Counting rate of selected Injun III detectors during revolution 994. Note correlation of auroral light output and particle downflux measured by 213C, 213D and EM.

Figure 17. Sample spectra observed during revolution 994. Note rapid increase toward lower energies.

Figure 18. Relation observed between the ratios of particle flux

$\frac{j(>10\ \mathrm{keV})\ /\ j(>40\ \mathrm{keV})}{j(>40\ \mathrm{keV})\ /\ j(>100\ \mathrm{keV})}$ during selected passes. The straight lines indicate the ratios to be expected if the spectra followed either a power-law or an exponential function. Various values of the corresponding shape parameters γ and E_o are indicated.

Figure 19. The ratios of Figure 18 shown as a function of satellite position south of the high latitude termination L_N.

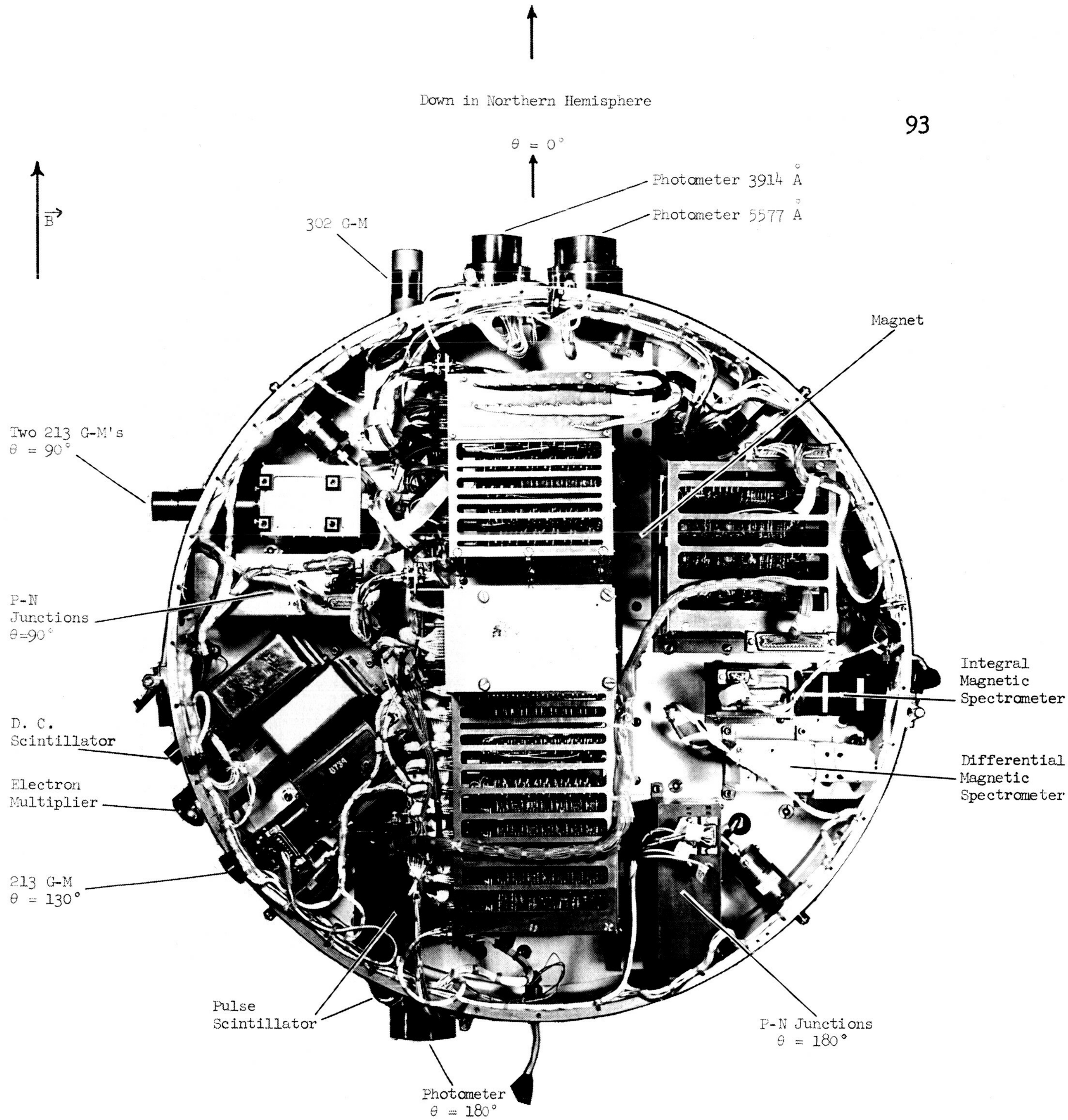
Down in Northern Hemisphere
$\theta = 0°$
$\vec{B}$
Photometer 3914 Å
Photometer 5577 Å
302 G-M
Magnet
Two 213 G-M's
$\theta = 90°$
P-N
Junctions
$\theta = 90°$
Integral
Magnetic
Spectrometer
D. C.
Scintillator
Differential
Magnetic
Spectrometer
Electron
Multiplier
213 G-M
$\theta = 130°$
Pulse
Scintillator
P-N Junctions
$\theta = 180°$
Photometer
$\theta = 180°$

Figure 1

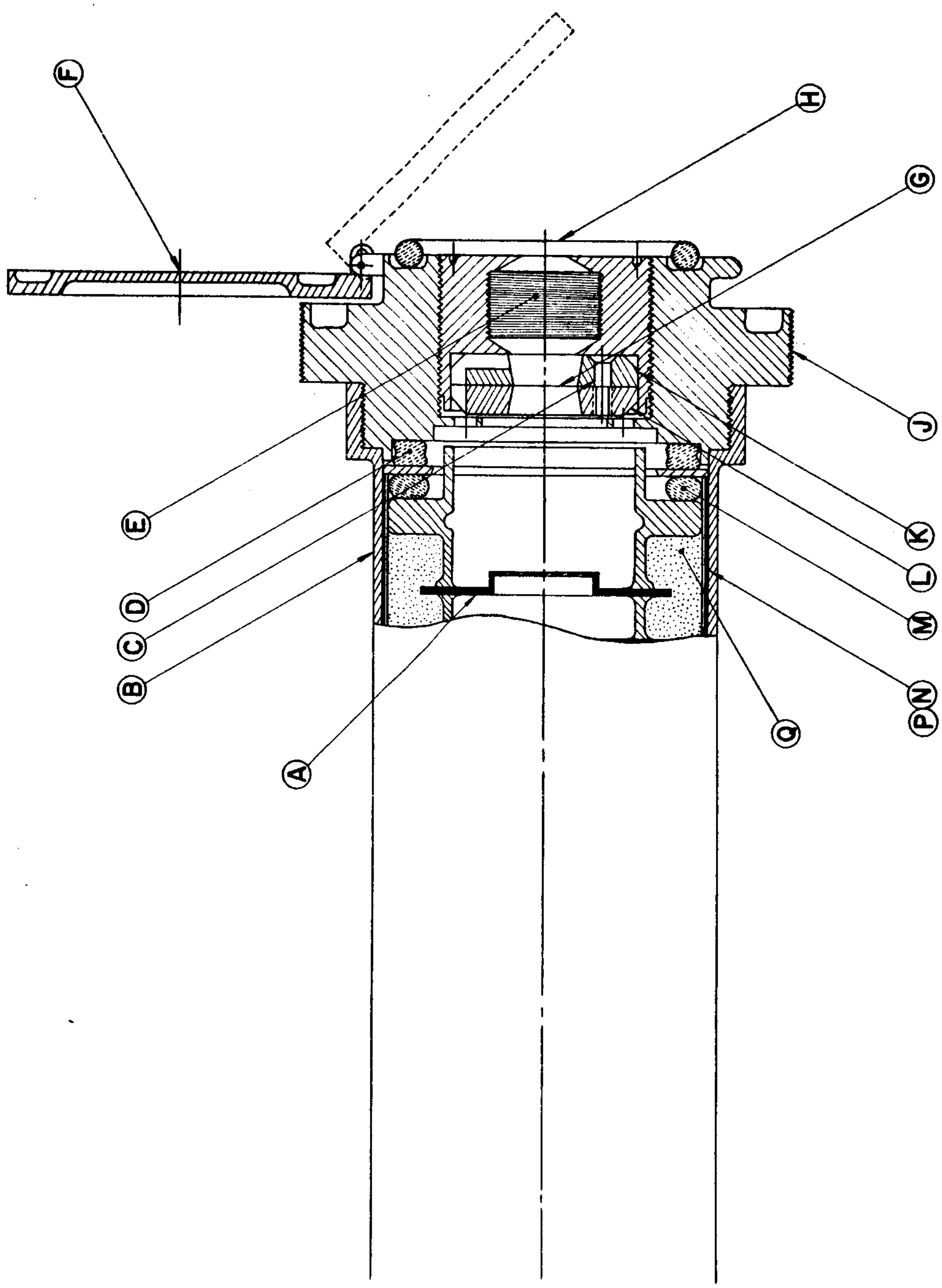

Figure 2

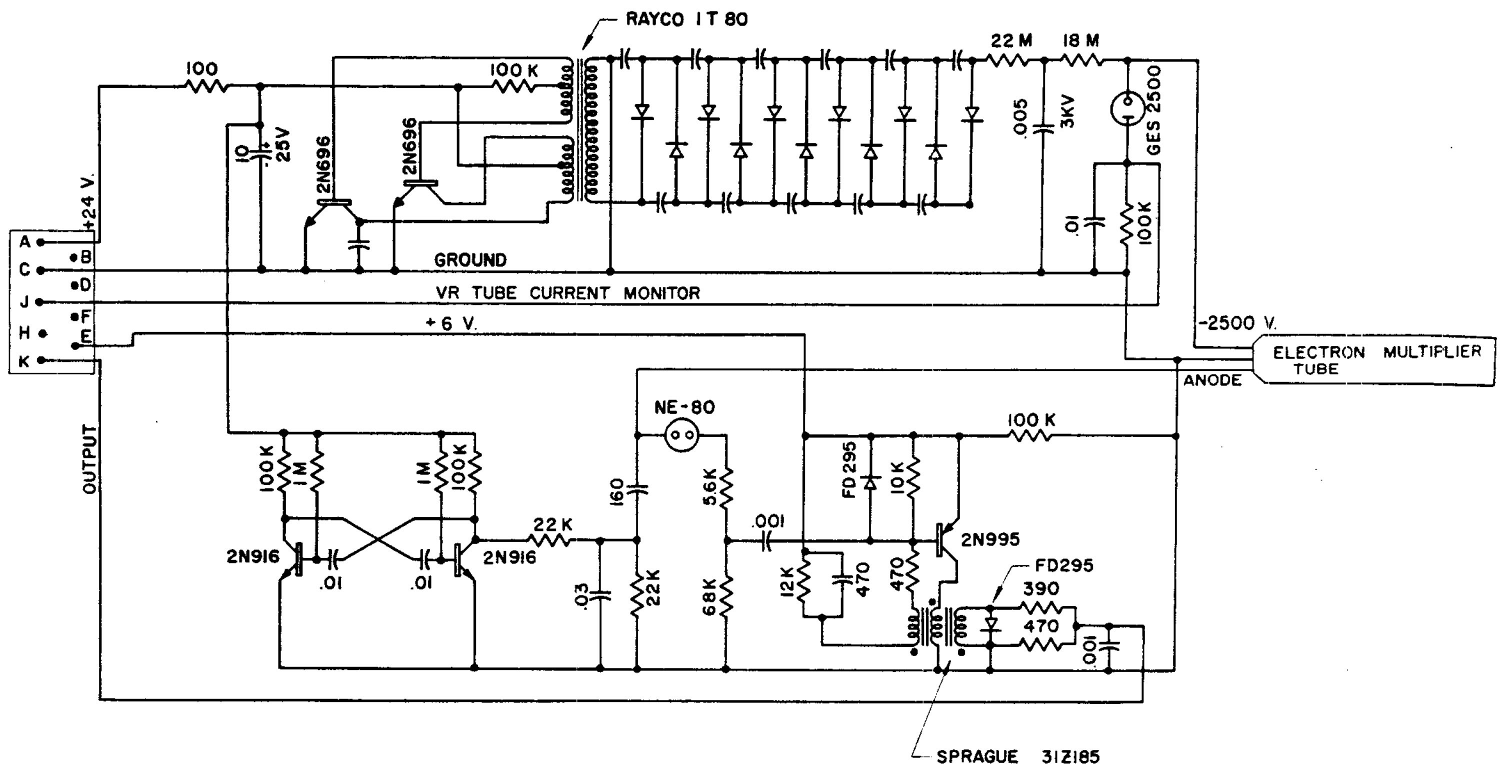

ALL DIODES MOTOROLA IN3283.
ALL CAPACITORS .003 UNLESS OTHERWISE SPECIFIED.

Figure 3

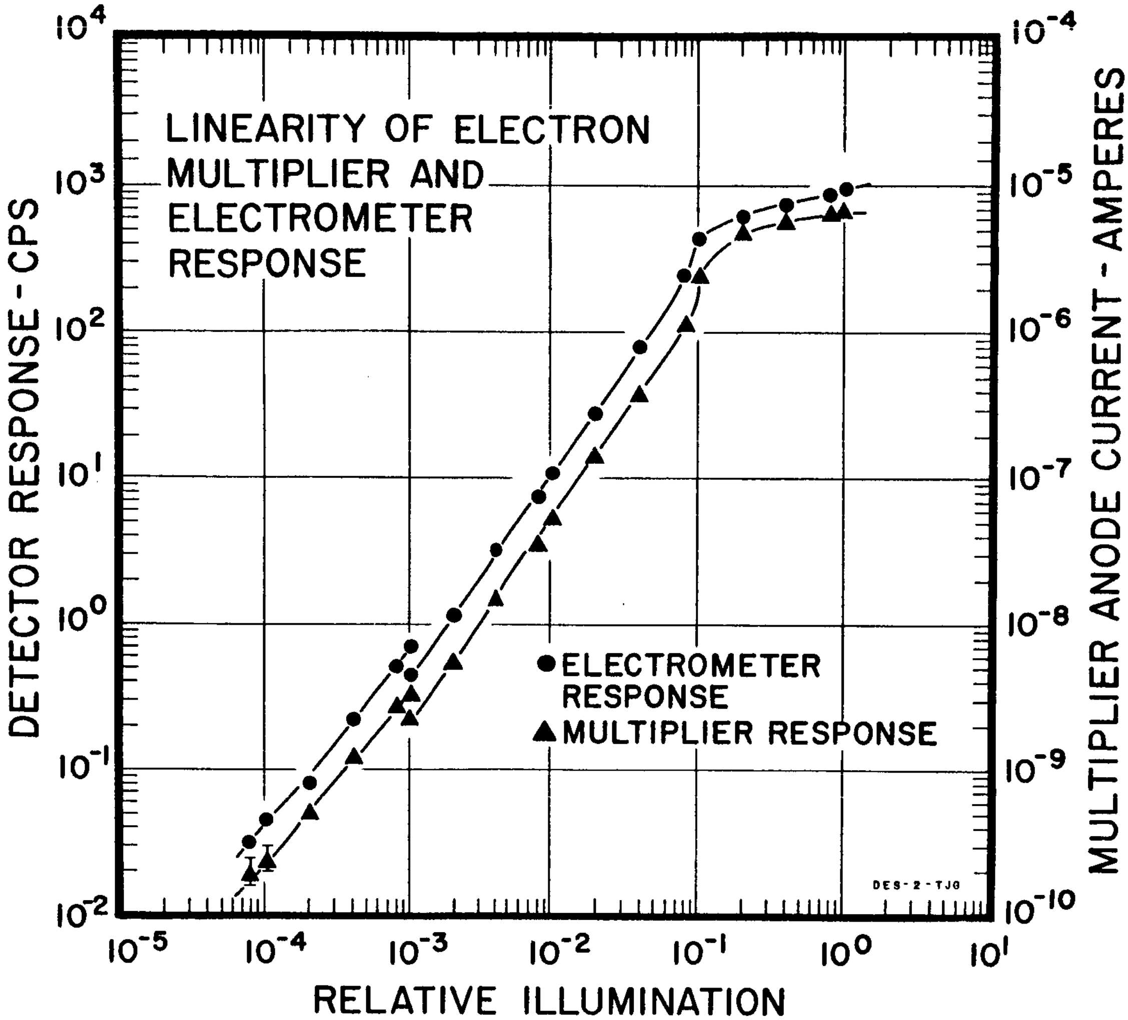

LINEARITY OF ELECTRON MULTIPLIER AND ELECTROMETER RESPONSE
DETECTOR RESPONSE - CPS
MULTIPLIER ANODE CURRENT - AMPERES
RELATIVE ILLUMINATION
ELECTROMETER RESPONSE
MULTIPLIER RESPONSE
DES-2-TJG
10^4
10^3
10^2
10^1
10^0
10^{-1}
10^{-2}
10^{-4}
10^{-5}
10^{-6}
10^{-7}
10^{-8}
10^{-9}
10^{-10}
10^{-5}
10^{-4}
10^{-3}
10^{-2}
10^{-1}
10^0
10^1

Figure 4

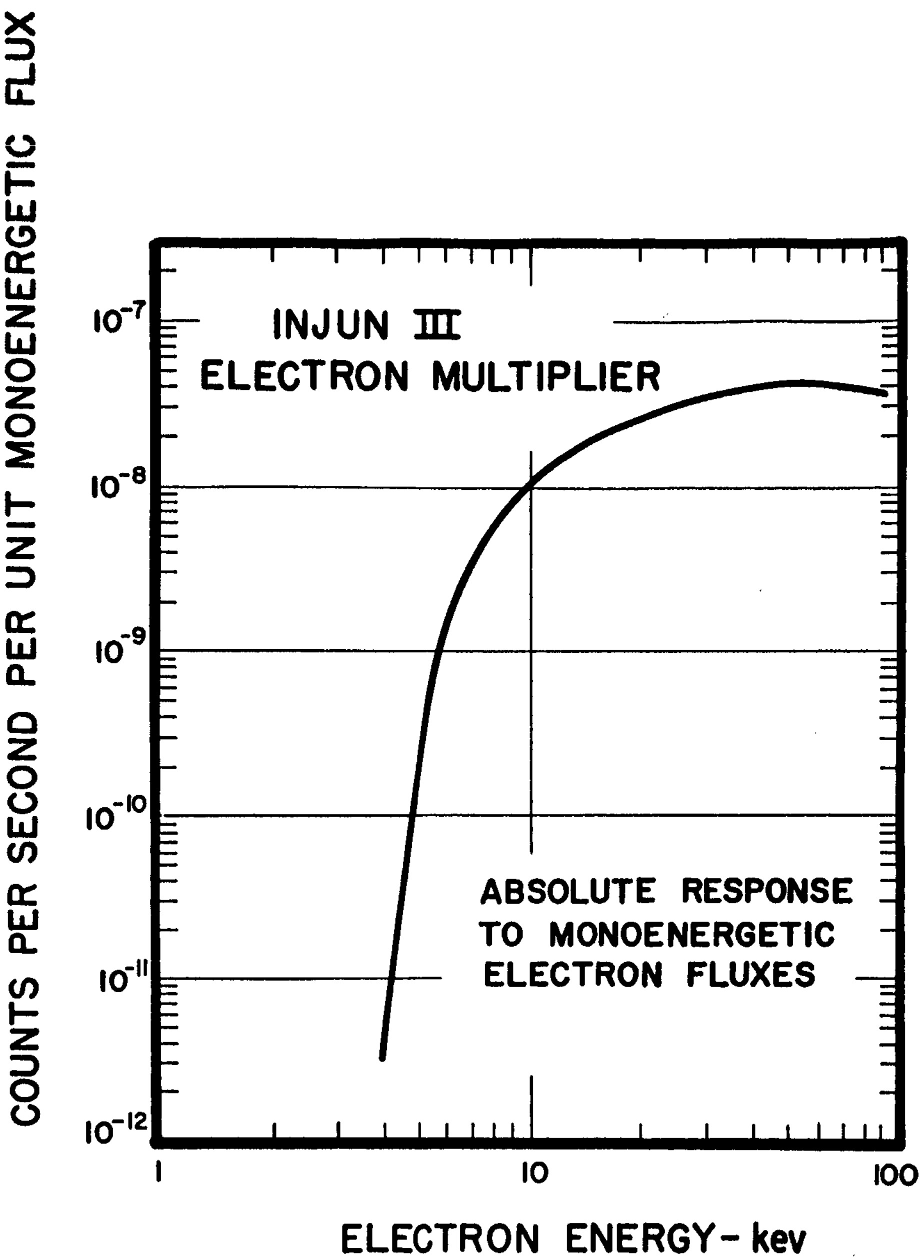
COUNTS PER SECOND PER UNIT MONOENERGETIC FLUX
INJUN III
ELECTRON MULTIPLIER
ABSOLUTE RESPONSE
TO MONOENERGETIC
ELECTRON FLUXES
10^{-7}
10^{-8}
10^{-9}
10^{-10}
10^{-11}
10^{-12}
1
10
100
ELECTRON ENERGY - kev

Figure 5

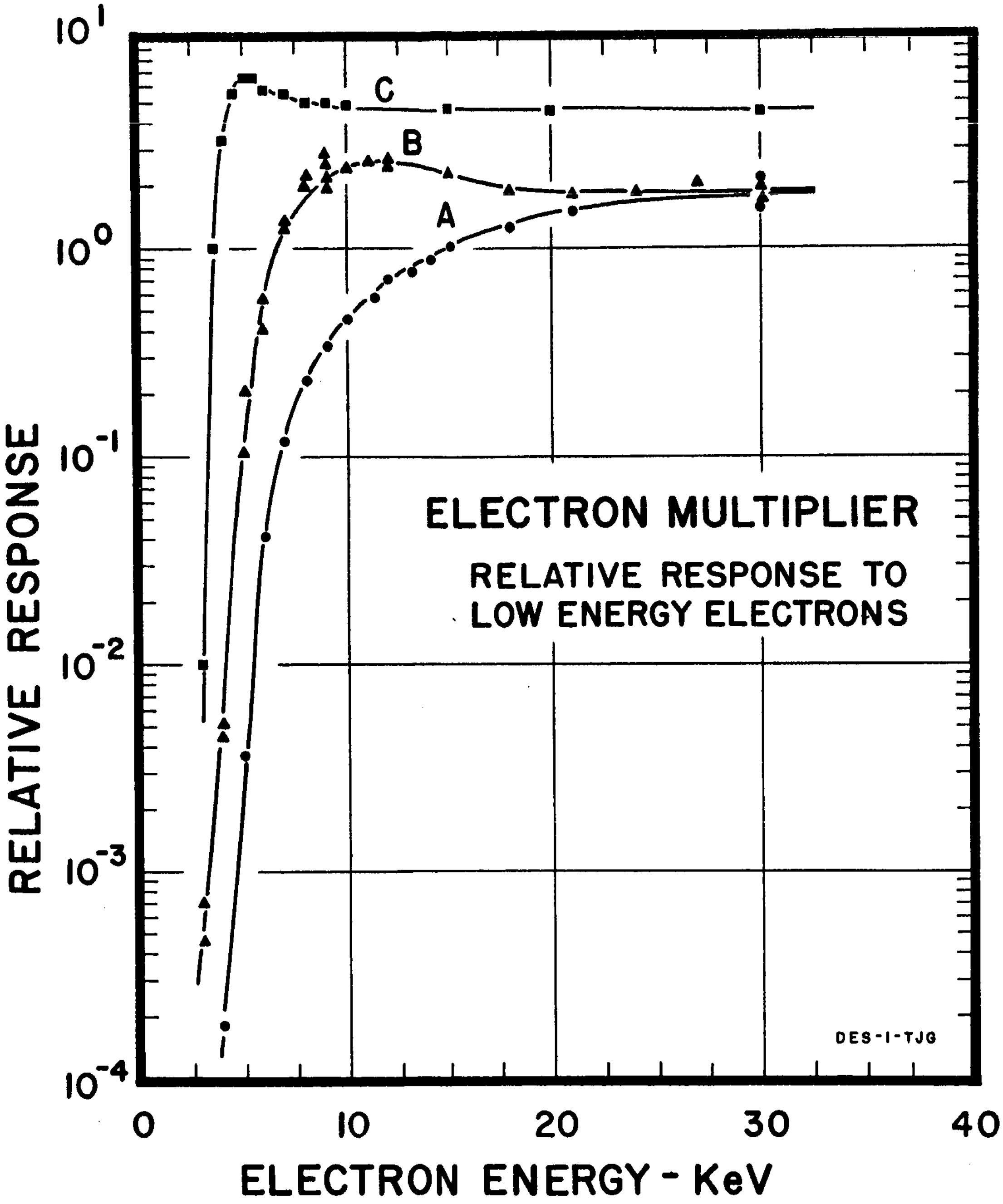

10^1
10^0
10^-1
10^-2
10^-3
10^-4
RELATIVE RESPONSE
C
B
A
ELECTRON MULTIPLIER
RELATIVE RESPONSE TO
LOW ENERGY ELECTRONS
DES-I-TJG
0
10
20
30
40
ELECTRON ENERGY - KeV

Figure 6

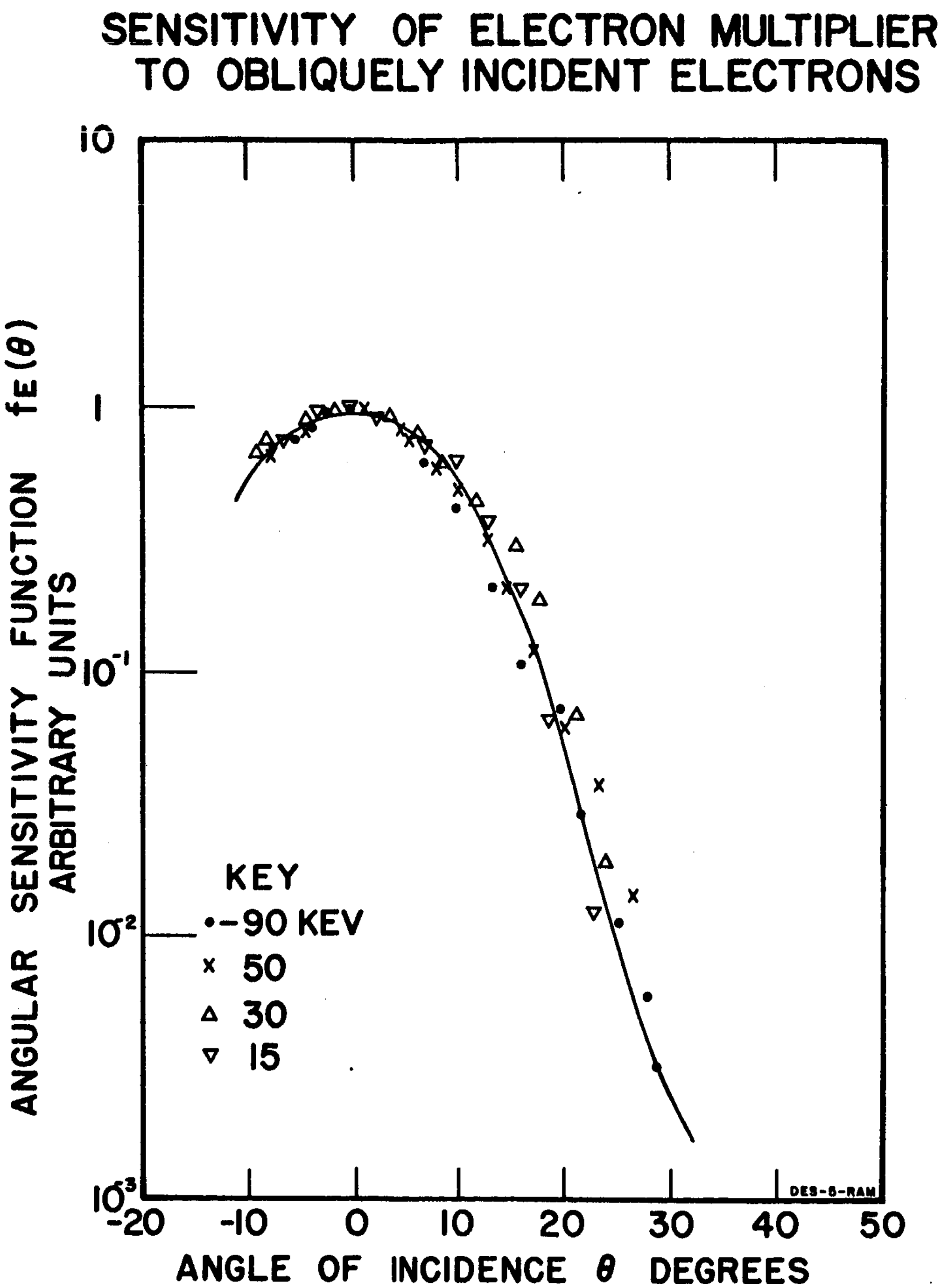
SENSITIVITY OF ELECTRON MULTIPLIER
TO OBLIQUELY INCIDENT ELECTRONS
ANGULAR SENSITIVITY FUNCTION fE(θ)
ARBITRARY UNITS
10
1
10⁻¹
10⁻²
10⁻³
KEY
•-90 KEV
× 50
△ 30
▽ 15
-20
-10
0
10
20
30
40
50
ANGLE OF INCIDENCE θ DEGREES
DES-6-RAM

Figure 7

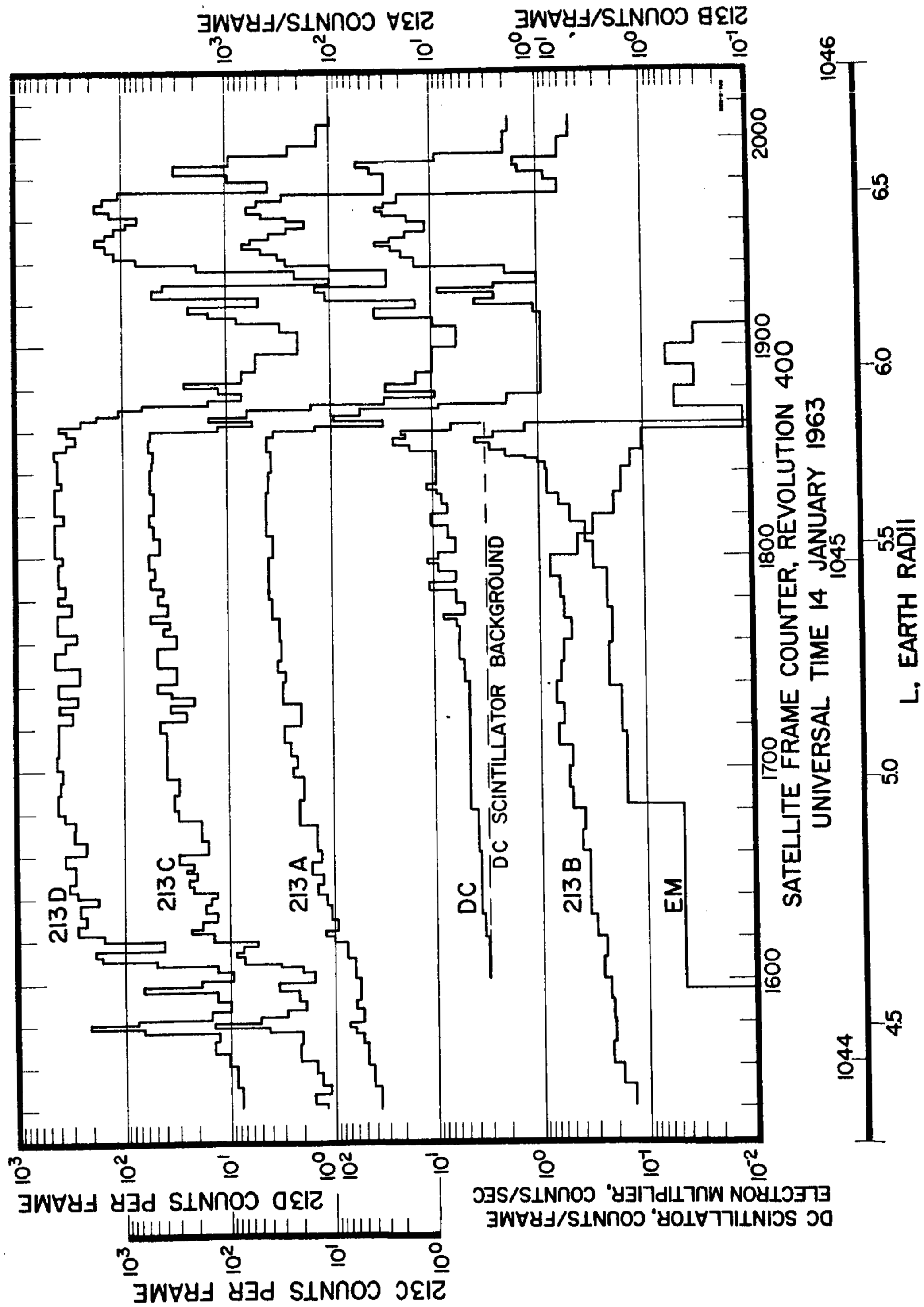
213D
213C
213A
DC
DC SCINTILLATOR BACKGROUND
213B
EM
213A COUNTS/FRAME
213B COUNTS/FRAME
213D COUNTS PER FRAME
213C COUNTS PER FRAME
DC SCINTILLATOR, COUNTS/FRAME
ELECTRON MULTIPLIER, COUNTS/SEC
1600
1700
1800
1900
2000
SATELLITE FRAME COUNTER, REVOLUTION 400
UNIVERSAL TIME 14 JANUARY 1963
1044
1045
1046
4.5
5.0
5.5
6.0
6.5
L, EARTH RADII

Figure 8

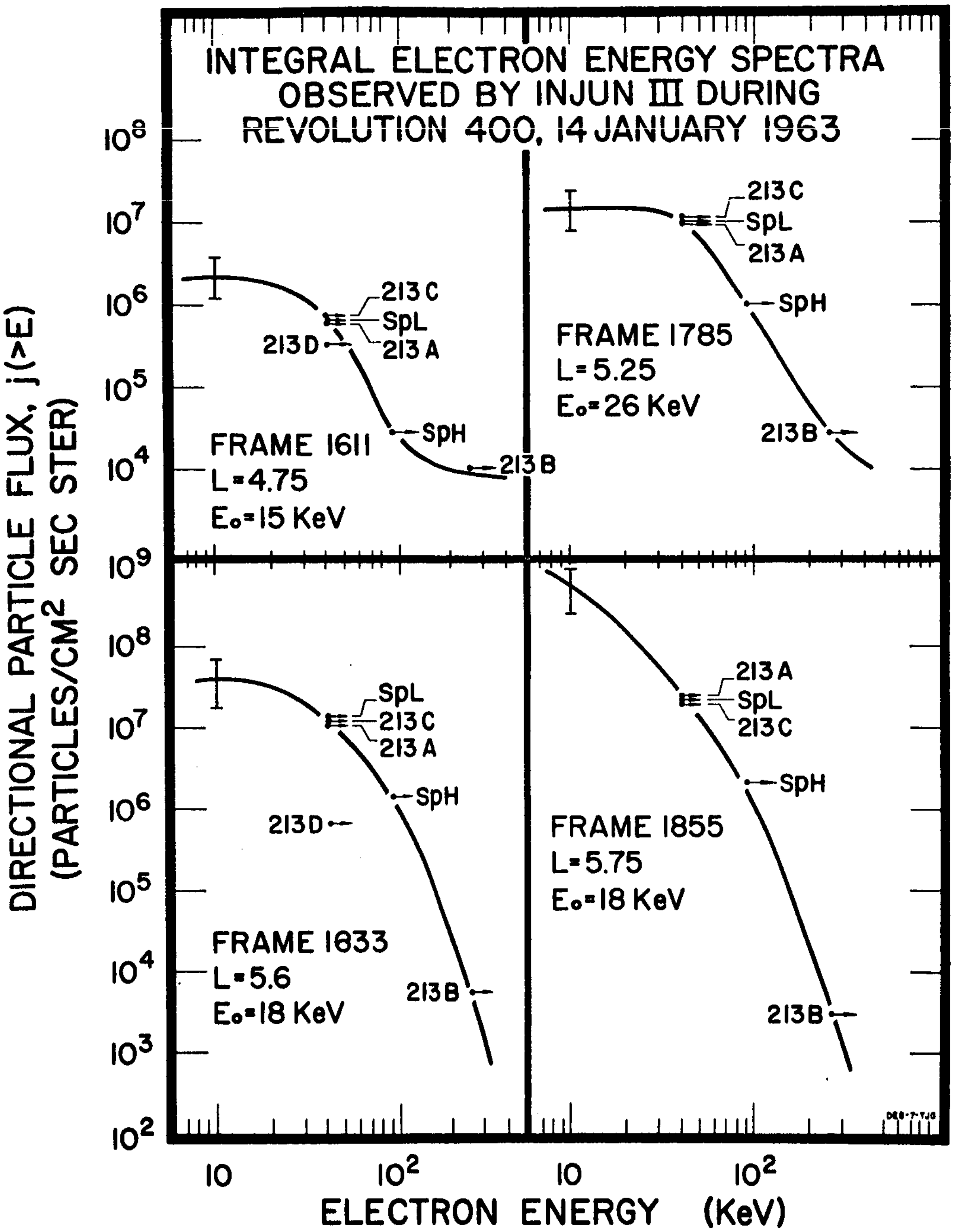
INTEGRAL ELECTRON ENERGY SPECTRA
OBSERVED BY INJUN III DURING
REVOLUTION 400, 14 JANUARY 1963
DIRECTIONAL PARTICLE FLUX, j(>E)
(PARTICLES/CM2 SEC STER)
FRAME 1611
L=4.75
Eo=15 KeV
FRAME 1785
L=5.25
Eo=26 KeV
FRAME 1833
L=5.6
Eo=18 KeV
FRAME 1855
L=5.75
Eo=18 KeV
213C
SpL
213A
213D
SpH
213B
ELECTRON ENERGY (KeV)

Figure 9

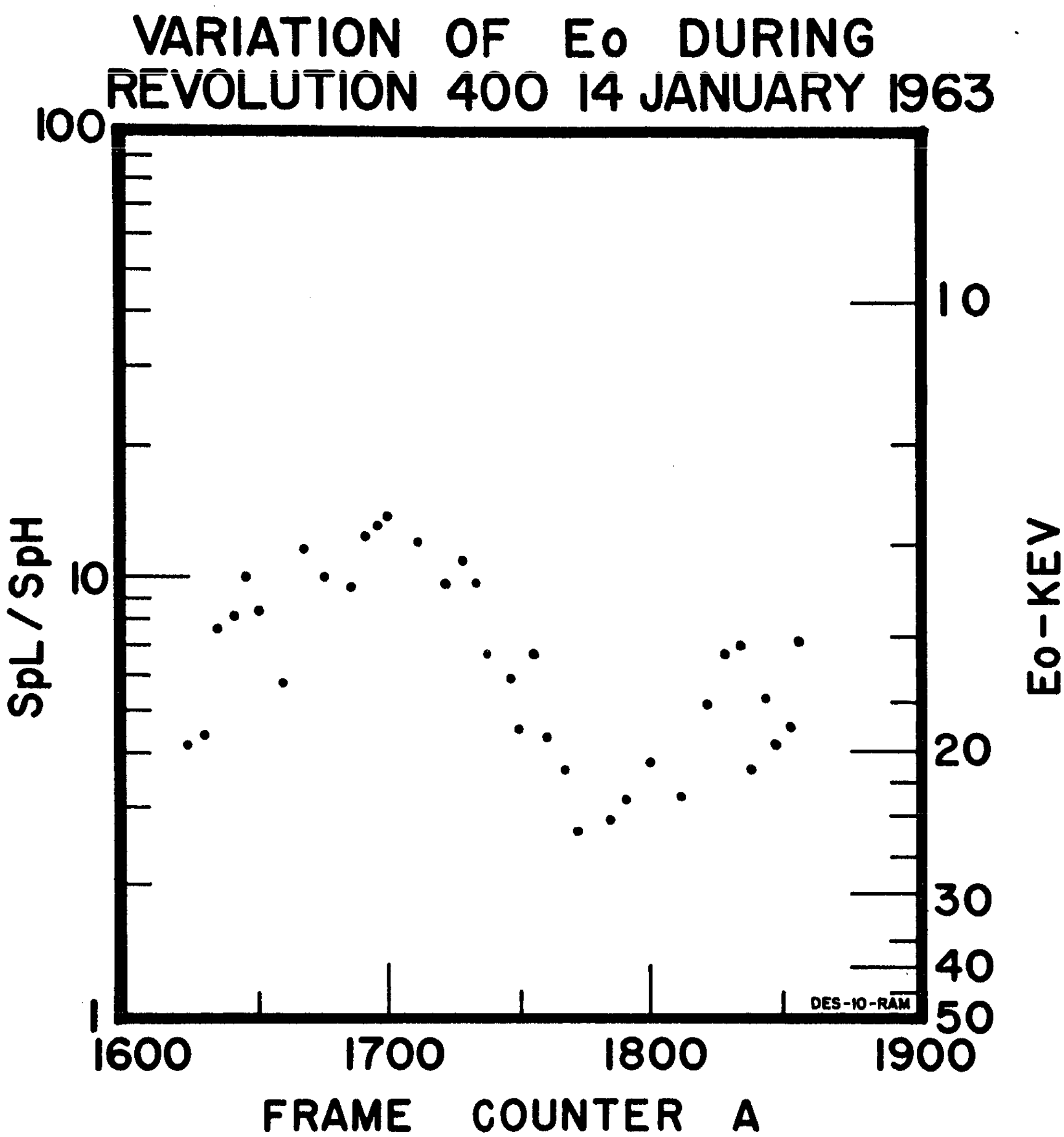
VARIATION OF Eo DURING
REVOLUTION 400 14 JANUARY 1963
100
10
1
SpL / SpH
10
20
30
40
50
Eo-KEV
DES-10-RAM
1600
1700
1800
1900
FRAME COUNTER A

Figure 10

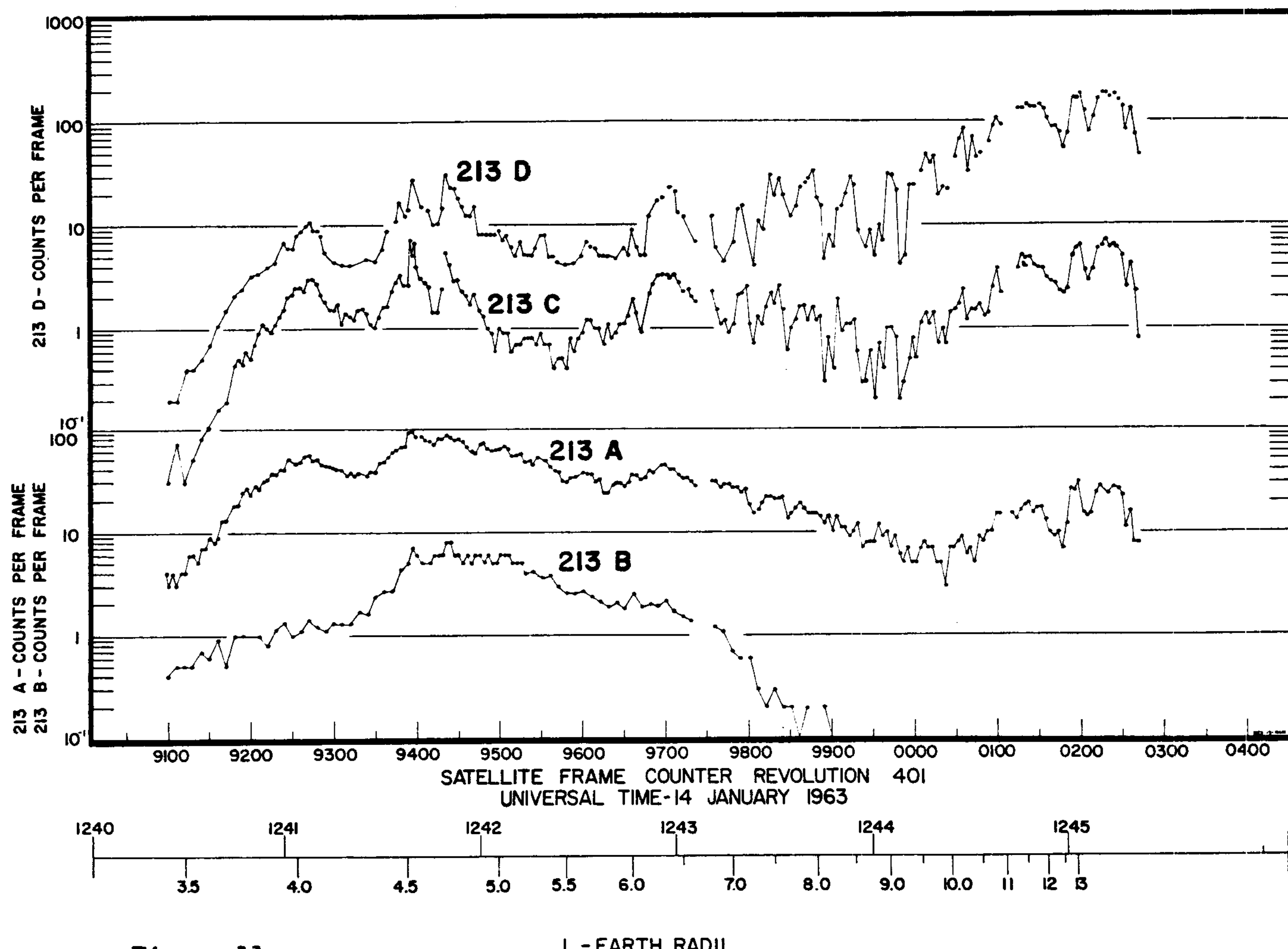
213 D
213 C
213 A
213 B
213 D - COUNTS PER FRAME
213 C - COUNTS PER FRAME
213 A - COUNTS PER FRAME
213 B - COUNTS PER FRAME
1000
100
10
1
10^{-1}
9100 9200 9300 9400 9500 9600 9700 9800 9900 0000 0100 0200 0300 0400
SATELLITE FRAME COUNTER REVOLUTION 401
UNIVERSAL TIME-14 JANUARY 1963
1240 1241 1242 1243 1244 1245
3.5 4.0 4.5 5.0 5.5 6.0 7.0 8.0 9.0 10.0 11 12 13
L - EARTH RADII

Figure 11

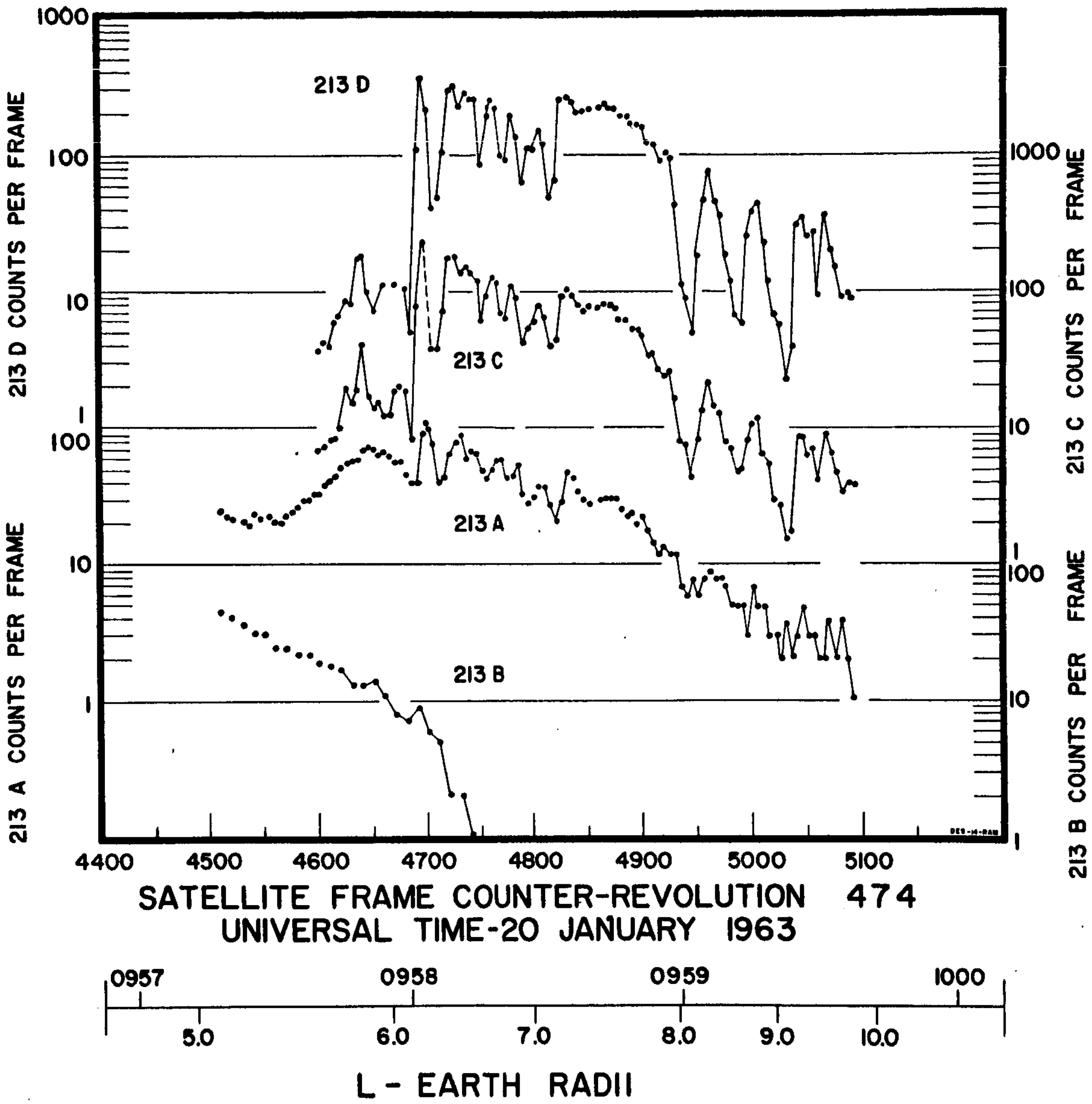
1000
100
10
1
100
10
1
213 D
213 C
213 A
213 B
213 D COUNTS PER FRAME
213 A COUNTS PER FRAME
1000
100
10
1
100
10
1
213 C COUNTS PER FRAME
213 B COUNTS PER FRAME
4400
4500
4600
4700
4800
4900
5000
5100
SATELLITE FRAME COUNTER-REVOLUTION 474
UNIVERSAL TIME-20 JANUARY 1963
0957
0958
0959
1000
5.0
6.0
7.0
8.0
9.0
10.0
L - EARTH RADII

Figure 12

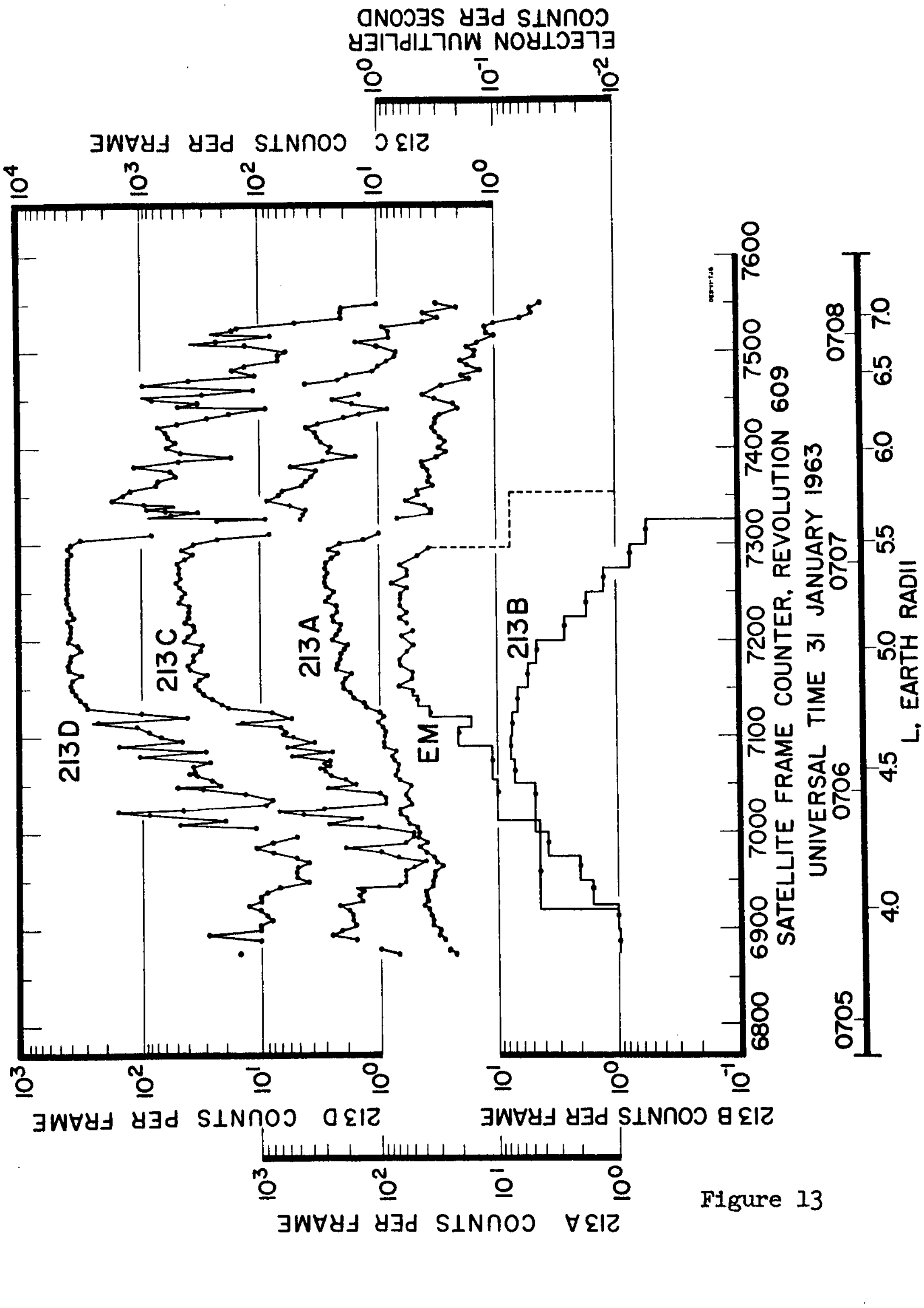
213 C COUNTS PER FRAME
ELECTRON MULTIPLIER COUNTS PER SECOND
213D
213C
213A
EM
213B
213 D COUNTS PER FRAME
213 B COUNTS PER FRAME
213 A COUNTS PER FRAME
SATELLITE FRAME COUNTER, REVOLUTION 609
UNIVERSAL TIME 31 JANUARY 1963
L, EARTH RADII

Figure 13

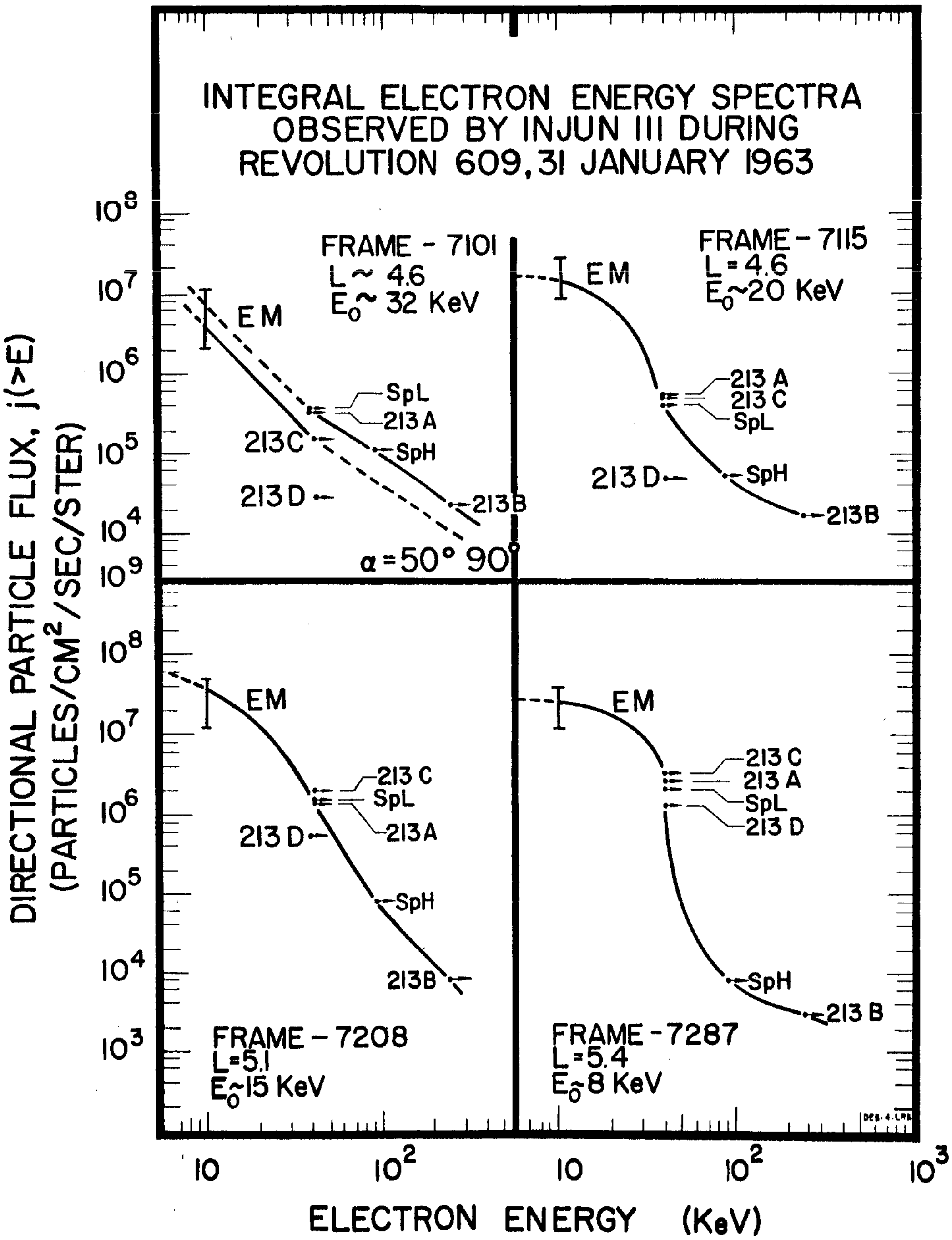

INTEGRAL ELECTRON ENERGY SPECTRA OBSERVED BY INJUN III DURING REVOLUTION 609, 31 JANUARY 1963
FRAME - 7101
L ~ 4.6
E0 ~ 32 KeV
FRAME - 7115
L = 4.6
E0 ~ 20 KeV
FRAME - 7208
L = 5.1
E0 ~ 15 KeV
FRAME - 7287
L = 5.4
E0 ~ 8 KeV
EM
SpL
SpH
213 A
213 B
213 C
213 D
α = 50° 90°
DIRECTIONAL PARTICLE FLUX, j(>E) (PARTICLES/CM²/SEC/STER)
ELECTRON ENERGY (KeV)

Figure 14

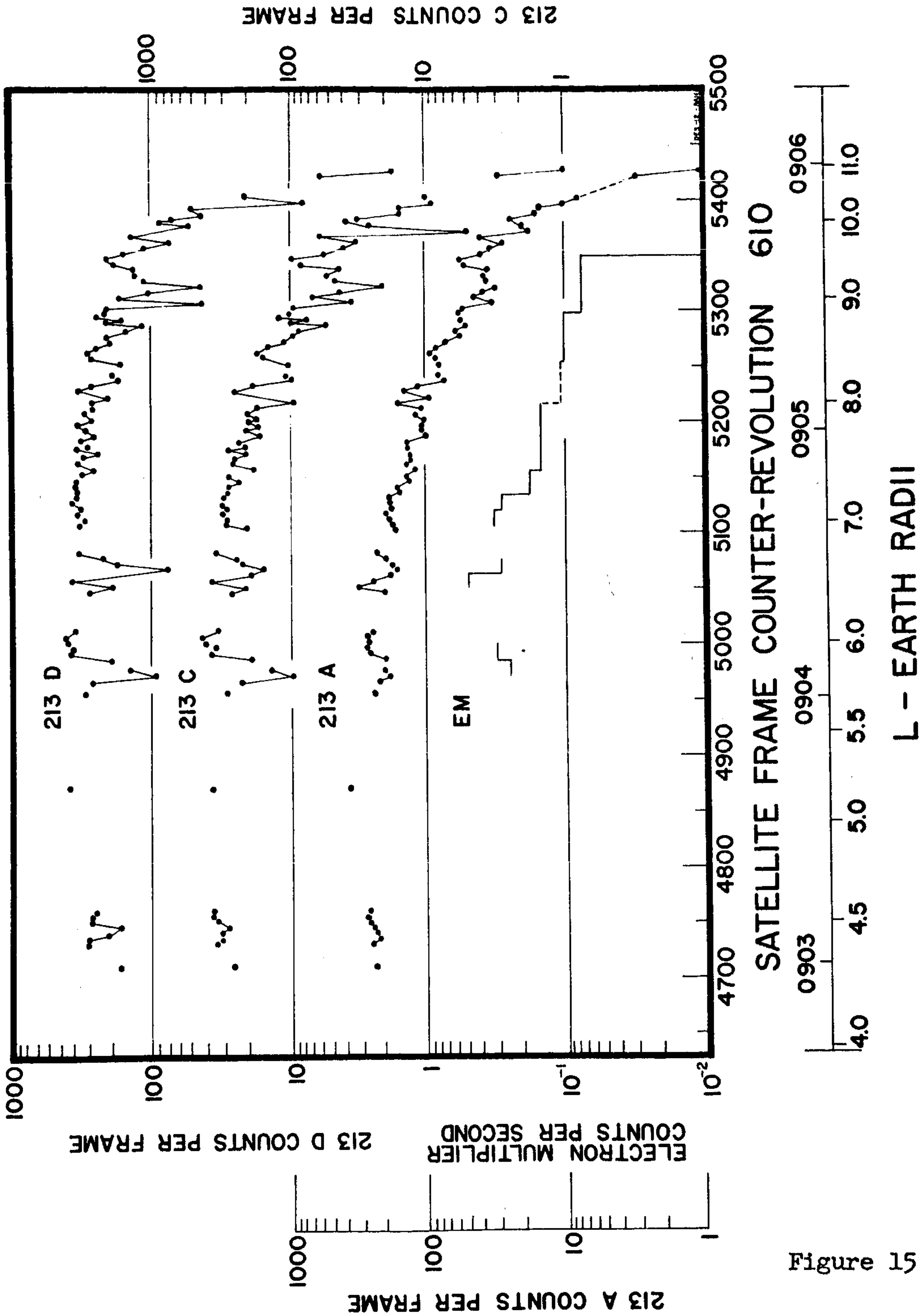
213 C COUNTS PER FRAME
213 D
213 C
213 A
EM
SATELLITE FRAME COUNTER-REVOLUTION 610
L - EARTH RADII
213 D COUNTS PER FRAME
ELECTRON MULTIPLIER COUNTS PER SECOND
213 A COUNTS PER FRAME

Figure 15

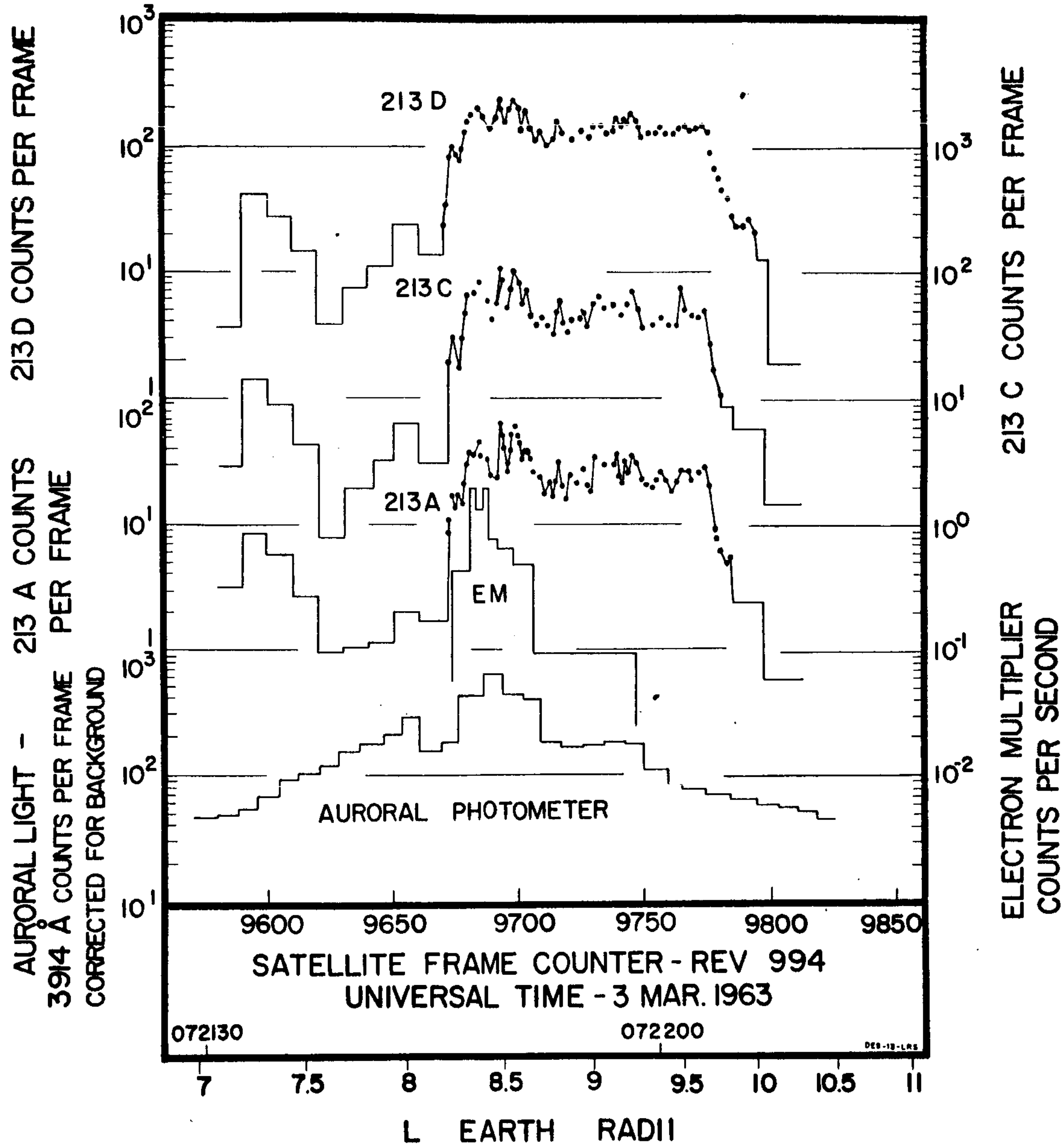
213 D COUNTS PER FRAME
213 A COUNTS PER FRAME
AURORAL LIGHT - 3914 Å COUNTS PER FRAME CORRECTED FOR BACKGROUND
213 C COUNTS PER FRAME
ELECTRON MULTIPLIER COUNTS PER SECOND
213 D
213 C
213 A
EM
AURORAL PHOTOMETER
9600
9650
9700
9750
9800
9850
SATELLITE FRAME COUNTER - REV 994
UNIVERSAL TIME - 3 MAR. 1963
072130
072200
7
7.5
8
8.5
9
9.5
10
10.5
11
L EARTH RADII

Figure 16

INTEGRAL ELECTRON ENERGY SPECTRA OBSERVED BY INJUN III DURING REVOLUTION 994 3 MARCH 1963

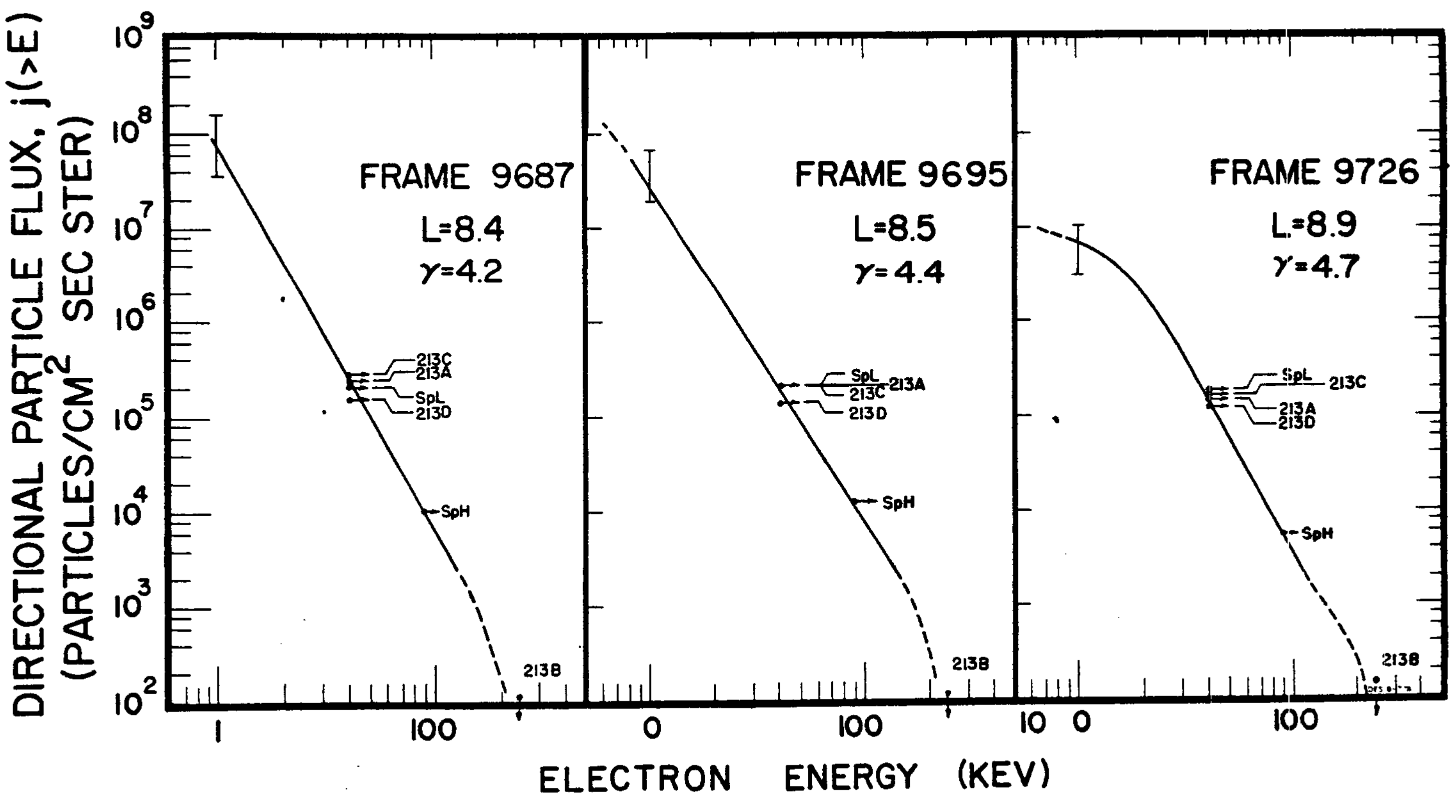

Figure 17

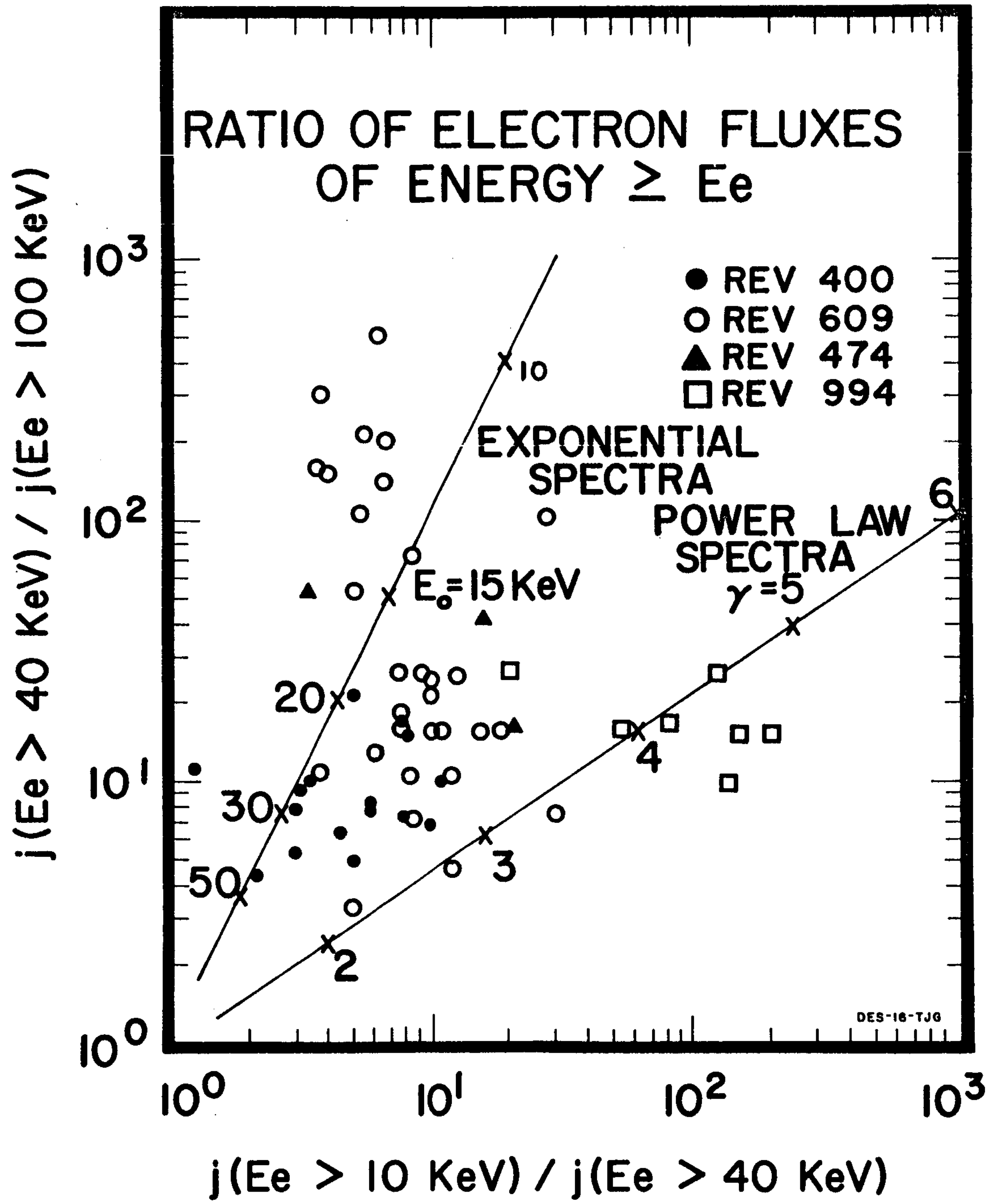
RATIO OF ELECTRON FLUXES
OF ENERGY ≥ Ee
● REV 400
○ REV 609
▲ REV 474
□ REV 994
EXPONENTIAL
SPECTRA
POWER LAW
SPECTRA
E₀=15 KeV
γ=5
10
20
30
50
2
3
4
6
DES-16-TJG
10^0
10^1
10^2
10^3
j(Ee > 40 KeV) / j(Ee > 100 KeV)
j(Ee > 10 KeV) / j(Ee > 40 KeV)

Figure 18

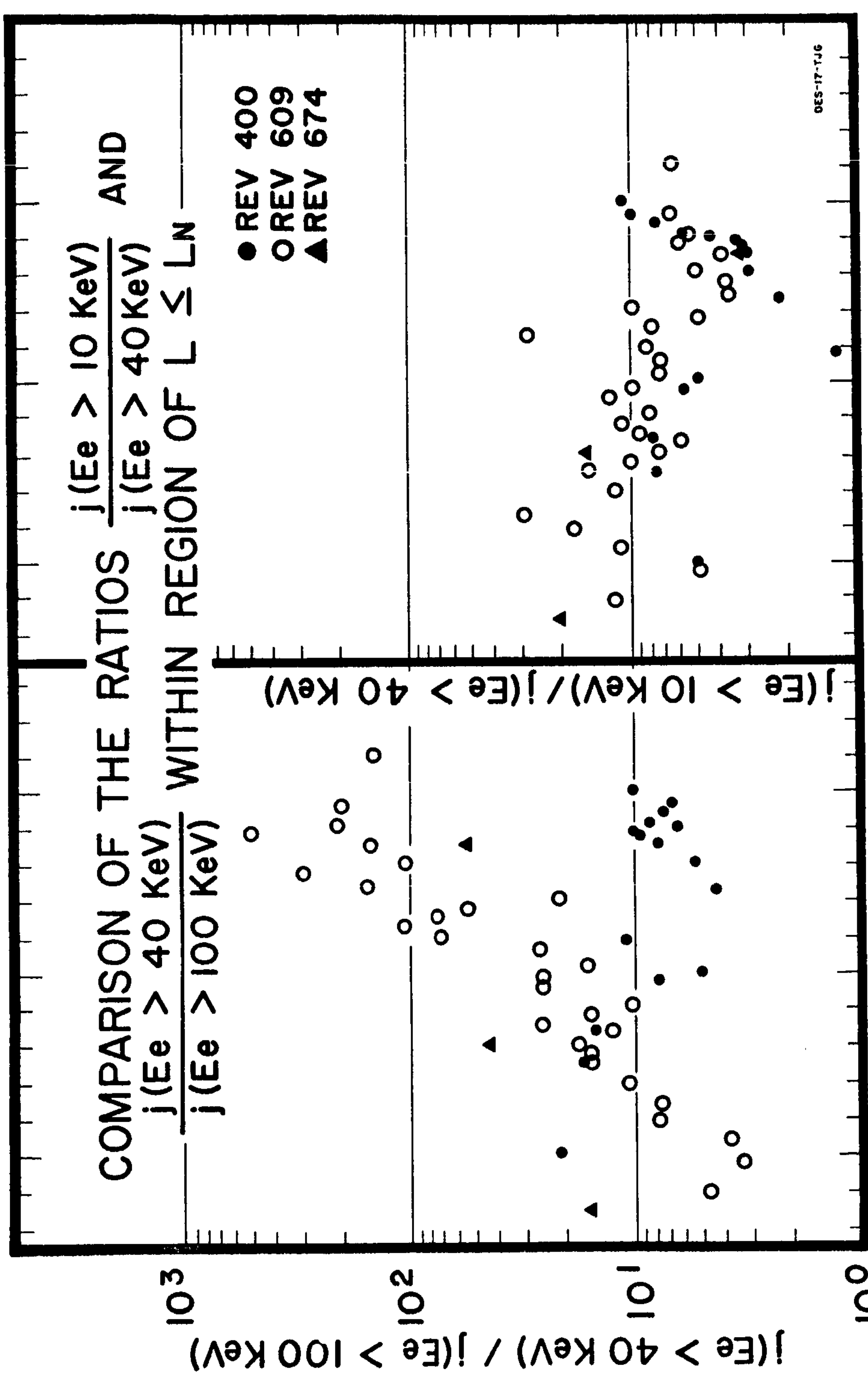
COMPARISON OF THE RATIOS j(Ee > 40 KeV) / j(Ee > 100 KeV) AND j(Ee > 10 KeV) / j(Ee > 40 KeV) WITHIN REGION OF L ≤ LN
● REV 400
○ REV 609
▲ REV 674
j(Ee > 40 KeV) / j(Ee > 100 KeV)
j(Ee > 10 KeV) / j(Ee > 40 KeV)
10^3
10^2
10^1
10^0
1.0
.5
0
-.5
LN - L
LN - L

Figure 19